Astron. Astrophys. 290, 69–103 (1994)

ASTRONOMY AND ASTROPHYSICS

The stellar population of the globular cluster M 3

I. Photographic photometry of 10 000 stars*

R. Buonanno[1], C.E. Corsi[1], A. Buzzoni[2], C. Cacciari[3], F.R. Ferraro[3], and F. Fusi Pecci[3]

[1] Osservatorio Astronomico di Monte Mario, Viale del Parco Mellini 84, I-00136 Roma, Italy
[2] Osservatorio Astronomico di Brera, Via Brera 28, I-20121 Milano, Italy
[3] Osservatorio Astronomico di Bologna, Via Zamboni 33, I-40124, Bologna, Italy

Received 17 December 1993 / Accepted 1 February 1994

Abstract. A new photographic colour-magnitude diagram (CMD) for the Galactic globular cluster M 3 is presented. This constitutes the preliminary part of a long-term project aiming at using the M 3 stellar population as a powerful testbench for the predictions of the stellar evolution theory and for cosmological purposes via the population synthesis methods.

In this first step, more than 10 000 stars were measured on the Mt. Palomar and Mt. Wilson original plates (Sandage 1953) down to $V > 21.5$ with very high internal accuracy to obtain complete samples over well defined areas. The list of magnitudes, colours and positions for all the measured stars is available from the CDS at Strasbourg upon request.

From the analysis of the present CMD the following results are derived: (a) The overall morphology of the main branches and their normal points reproduce in essence the previous results. In particular, the existence of a sizeable population of *blue straggler stars* (BSS) detected by Sandage (1953) is confirmed. (b) The Red Giant Branch (RGB) and Asymptotic Giant Branch (AGB) are clearly separated, and the RGB metallicity indicators lead to $\langle[Fe/H]\rangle = -1.66 \pm 0.10$ with an upper limit $\sigma[Fe/H] \sim 0.09$. The narrow Sub-Giant Branch (SGB) and Turn-Off (TO) region suggest that also the dispersion in the abundance of C,N,O should be very low. (c) The Horizontal Branch (HB) is narrow and the bulk of HB stars covers a wide range in effective temperature ($\log T_e = 3.70$ to 4.55). Six groups of stars have been tentatively identified based on their location on the HB, namely: R (red), V (variables), B (blue), EB (extremely blue) HEB (hot extremely blue) ER (extremely red) – some of these stars may be non-genuine HB stars. The various population ratios computed lead: *(i)* to confirm the full extension of semiconvection (or, alternatively, to calibrate the overshooting parameter) and to exclude the existence of a "long" *breathing pulses* phase; and *(ii)* to determine the primordial helium abundance Y_p via the R-method, $Y_p = 0.23 \pm 0.02$. (d) The distance modulus is estimated as $(m - M)_0 = 14.94$ and the age is $t = 18.7 \pm 3.5$ Gyr. The effects of different assumptions and the results previously obtained by various authors using the present data are also discussed. It is interesting to note the wide range of values estimated for the age (from $\sim$ 13 to $\sim$ 20 Gyr). (e) 65 BSS candidates have been identified. Within the considered areas, BSS seem to be less centrally concentrated than the subgiants in the same magnitude interval, but further checks are needed. Speculations on the possible detection of a BSS progeny located in the red HB are also presented.

Future papers of this series will deal with the analysis of CCD data for the inner regions of the cluster.

Key words: globular clusters: M 3 – HR diagram – stars: evolution

1. Introduction

The availability of globular cluster colour-magnitude diagrams (CMDs) and luminosity functions (LFs) obtained with very high photometric accuracy from *very populous* and *complete* samples of stars still represents the most powerful tool to provide sensitive tests for the theory of stellar evolution of low-metallicity, low-mass stars (Renzini & Fusi Pecci 1988).

The main requirement to fulfil in order to compare the predictions of the models with the observable parameters is the existence of *statistically significant* samples of stars evolving along the considered evolutionary path. The shorter is the phase to study, the larger must be the surveyed sample. The smaller are the predicted features in the various branches of the CMD, the more precise must be the photometric measures.

Given the tremendous progress in the theoretical understanding of stellar evolution in globular clusters, and the perspective of using clusters as templates in studying the evolution of stellar populations in galaxies, it is now clear that only *very big and very accurate* samples may allow to achieve a decisive

Send offprint requests to: F. Fusi Pecci

* Tables 4 and 6 are only aviable in electronic form. See the Editorial in A&A, 1993, Vol. 280(3), p. E1

improvement in the comparison between theoretical models and observations.

An optimal photometric study would thus include for instance a *complete, wide survey* with a CCD-camera out to the outskirts of many clusters (purposely chosen to span proper ranges in metallicity, intrinsic structural properties, galactocentric distances, etc.), coupled with a few exposures with the *Wide Field Planetary Camera* of the *Hubble Space Telescope* (HST) to resolve all the stars down to the turn-Off (TO) in the central regions, and possibly pick up a well representative sample of the cluster white dwarf population. We have planned already some years ago a long-term project to pursue this aim, but the space data are not available yet because of the well known problems with HST. On the other hand, until the recent availability of new large format CCD's, also the complete homegeneous coverage of the clusters from the ground was not an easy task to accomplish.

As a first step towards the achievement of this global goal, in 1984 we decided to start a pilot project focussed on the Galactic globular cluster M 3 = NGC 5272, a classical prototype for the Population II stars. In essence, we planned to re-measure all the stars in the set of original plates taken by Sandage (1953) and used to obtain the first CMD of M 3. A large number of photometric and spectroscopic studies have been carried out on this cluster after those early measurements, but no complete photometric survey is available yet.

We are of course aware that the use of photographic plates may lead to a worse photometric accuracy with respect to CCD data, but the availability of many plates per colour (at various exposure levels) and the possibility of using a good semi-automatic package for photometric data reduction (ROMAFOT, Buonanno et al. 1979, 1983b) led us to conclude that this photometric study was worth the effort. Eventually, more than 10 000 stars were measured, most of them with internal photometric errors less than 0.05 mag even at $V \sim 21$ (about two mag fainter than the turnoff), and complete and populous samples were obtained for all the main post-Main-Sequence branches. This result represents a significant improvement with respect to Sandage (1953) both in terms of photometric accuracy and completeness (see Sects. 2.3 and 2.4).

This paper presents the data we obtained from this 1984 photometric study, which we believe are still worth publication as they have been quite frequently referred to in the subsequent years, and may still represent a basic tool for the many researchers interested in the study of the stellar population of this important cluster.

Preliminary presentations of this CMD of M 3 were already given in the past years (Buonanno et al. 1986, 1988; Renzini & Fusi Pecci 1988). Future papers in this series, based on new BVI CCD data of the innermost regions, will deal with the photometry of about 9000 constant and 65 variable stars (Ferraro et al. 1994; Cacciari et al. 1994), and the new detection of about 50 bright Blue Straggler Stars (BSS) (Ferraro et al. 1993). Also a new JHK photometric study will be presented (Guarnieri et al. 1990, 1994), and, finally, a detailed study of the Luminosity Functions for individual branches and for the global samples in various colours and in bolometric luminosity, with particular emphasis on model testing and population and spectral synthesis methods (Buzzoni et al. 1994a).

Section 2 is devoted to the description of the data acquisition and treatment. The properties of the CMD are presented and discussed in Sect. 3 and in Sect. 4 we briefly discuss the blue straggler candidates detected in these external areas. For a specific analysis of the whole BSS sample (including also those we recently detected in the inner regions from CCD data) we refer to Ferraro et al. (1993).

2. Observations, reductions and data

2.1. Observations and reductions

To obtain a deep and complete CMD for M 3, we used the set of photographic plates taken in the early fifties at Mt. Palomar and Mt. Wilson Observatories (Sandage 1953). A complete description of the photographic material can be found in Table 1.

A square region of about $14' \times 14'$ centered on the cluster was scanned with the PDS machine at ESO, Garching. The PDS was used in density mode with a 25 μm square aperture and a 20 μm step. The data were smoothed by a 3×3 pixel weighted convolution mask and then transformed into relative counts using for each plate an empirically derived calibration curve. Then, the digital images were analysed using the photometric reduction package ROMAFOT, which was developed for stellar photometry in crowded fields by Buonanno et al. (1979, 1983b). Briefly, the technique consists in using the experimental point spread function (PSF) to reconstruct the stellar images via a multi-peak two-dimensional fit. The luminosity of the sky background is shaped with an inclined plane. Further details on the reduction algorithms and procedures can be found in some papers published by our group (e.g. Buonanno et al. 1983a; Buonanno & Iannicola 1988; Ferraro et al. 1990, 1992a,b,c).

2.2. Magnitudes, colours and positions

All the stars in an annulus with distance $3.5' < r < 6'$ from the cluster centre (see Fig. 1 **area I**, hereafter **AI**) were measured down to $V > 21.5$. The "completeness" of the sample was ensured (see Sect. 2.4) by selecting the annulus location appropriately, so as to minimize the crowding problems that affect the innermost regions, and the field contamination problems that become significant in the most external regions of the cluster.

To increase the statistical significance of the population of the various evolved branches, we also measured all the stars external to the considered annulus (i.e. with $r > 6'$) over a square region $\sim 14' \times 14'$ (**area II**, hereafter **AII** in Fig. 1) down to $B \leq 18.6$, which we trust to be the limit of the Blue HB tail. A third sample of stars (also complete down to $B < 18.6$) was finally measured in an inner annulus ($2' < r < 3.5'$, **area III**, hereafter **AIII**, in Fig. 1).

In conclusion, the sample is complete down to $B < 18.6$ (see Sect. 2.4) over a region merging AI + AII + AIII (a square $\sim 14' \times 14'$ minus a central circle with radius $r = 2'$, see Fig. 1),

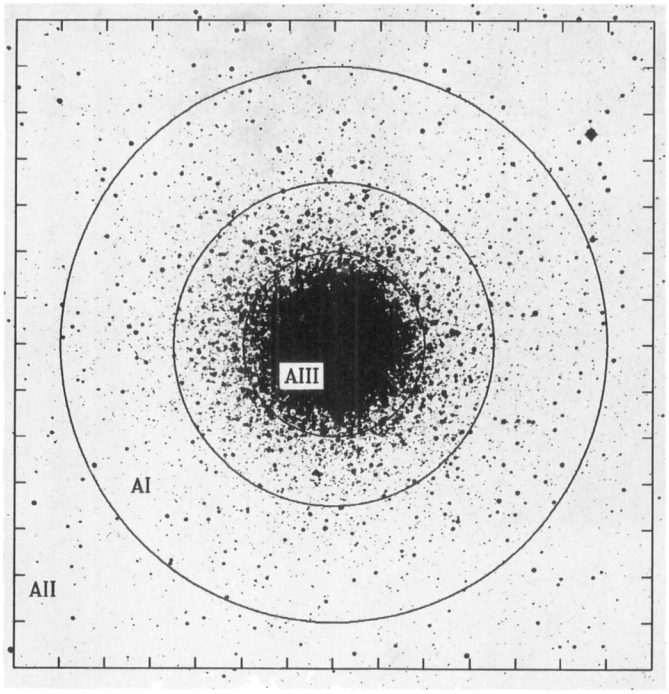

Fig. 1. Map of the surveyed regions in M 3. In area **AI**, with radial distance $3.5' < r < 6.0'$, all the stars were measured down to $V > 21.5$. In the inner annulus **AII** with $2.0' < r < 3.5'$, and in the $14' \times 14'$ external square **AIII** with $r > 6.0'$, the magnitude limit for completeness is $B = 18.6$ (see text). This study does not include measurements for stars with $r < 2.0'$

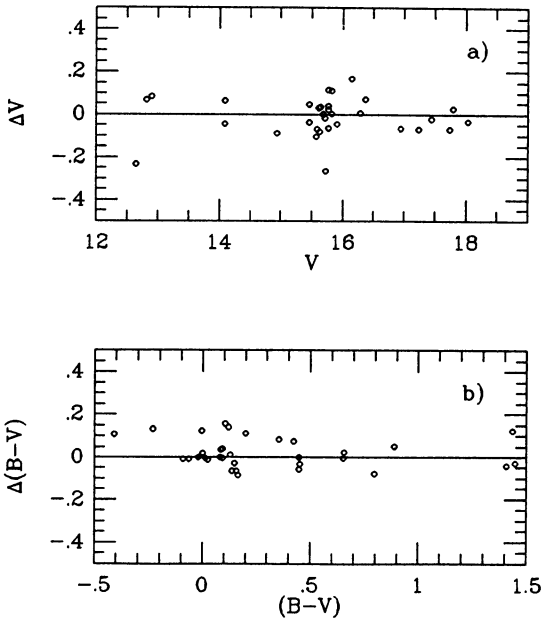

Fig. 2a and b. Calibration curves using the available bright photoelectric standards from Sandage (1970)

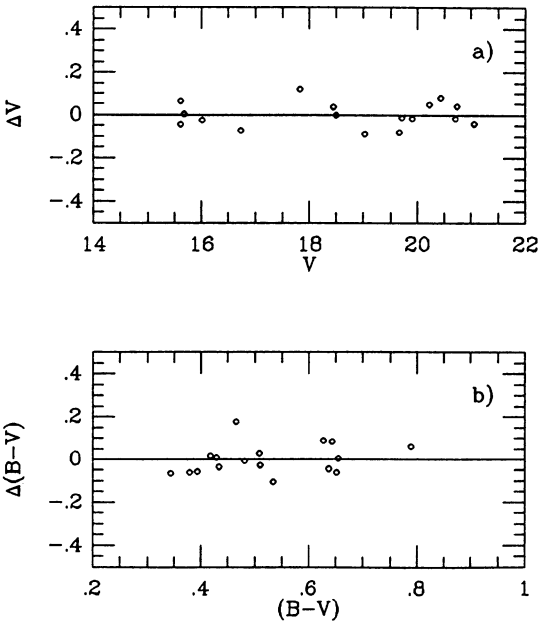

Fig. 3a and b. Magnitude and colour residuals for the faint standards (Sect. 2.2)

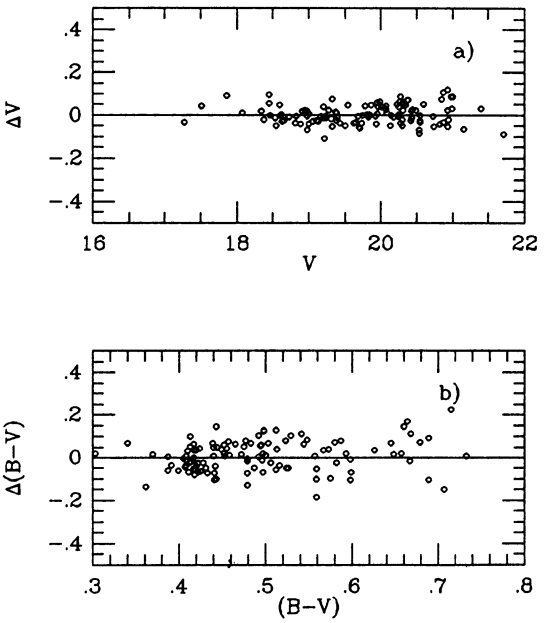

Fig. 4a and b. Magnitude and colour residuals for the faint "secondary" standards in the "transfer area" (Sect. 2.2)

while completeness for fainter stars (down to about $V \sim 21.5$) has been attained only in the region AI ($3.5' < r < 6'$).

In the reduction procedure the PSF for each plate was first determined and then the magnitudes in arbitrary units were derived. The magnitude indices ($-2.5 \log V_i$, where V_i is the volume of the ith element) derived for each plate were transformed into a "standard plate" in each colour and then averaged using appropriate weights.

Table 1. Observational material

Plate no.	Date	Emulsion+filter	Exp. time (min.)	FWHM (arcsec.)	Telescope
H 90 S	May 2 1951	103aO+WG2	20	1.5	100 inch [a]
H 91 S	May 2 1951	103aD+GG11	60	1.6	100 inch [a]
H 109 S	May 4 1951	103aO+WG2	30	1.5	100 inch [a]
H 110 S	May 4 1951	103aD+GG11	60	1.3	100 inch [a]
H 237 S	April 14 1953	IIaO+WG2	15	1.3	100 inch [a]
H 246 S	April 15 1953	103aD+GG11	15	1.2	100 inch [a]
PH 377 B	June 1 1951	103aO+GG1	25	1.5	200 inch [b]
PH 379 B	June 1 1951	103aD+GG11	65	1.4	200 inch [b]
PH 383 B	June 2 1951	IIaO+GG1	25	0.9	200 inch [b]
PH 385 B	June 2 1951	103aD+GG11	50	0.8	200 inch [b]
PH 392 B	June 3 1951	IIaO+GG1	25	1.3	200 inch [b]
PH 393 B	June 3 1951	103aD+GG11	50	1.5	200 inch [b]
PH 4507 S	April 13 1964	103aO+GG13	20	0.8	200 inch [b]
PH 4518 S	April 14 1964	103aD+GG11	30	1.0	200 inch [b]

[a] Diaphragmed to 58 inches.
[b] With the Ross f 3.67 corrector lens.

The calibration to the B,V Johnson system was obtained using the sequence of photoelectric standards available in the field (Sandage 1970) and reported in Table 2. To match the derived magnitude scale to the photoelectric sequence a polynomial fitting was adopted for the stars brighter than $V \sim 18$. The calibration of the faint stars was made difficult by the insufficient number of photoelectric standards in AII. The available standards in fact lie in a region north to the cluster, outside most of the area covered by the plates used in the present study. We have thus used an appropriate set of plates to define magnitude transfers via a populous photographic secondary sequence in common between the two areas. Figures 2a,b, 3a,b and 4a,b show the comparison between Sandage's original data and those obtained via the described procedure for the standard stars in two magnitude ranges. The accuracy of magnitudes and colours is discussed in detail in Sect. 2.3.

Fairly accurate positions are also a natural product of our fitting procedure. The coordinates X,Y (in arcsec) with respect to the cluster centre $\alpha_{1950} = 13^h39^m54^s$ and $\delta_{1950} = +28°38'$) were derived in the local system in each measured plate, and then transformed to a "standard plate" and converted to Cudworth's (1979) grid using a polynomial transformation by means of 55 common stars whose membership probabilities exceed 99%. Typical errors for the *relative* positions of the unblended objects should be lower than 0.05 arcsec.

Three samples of measured stars are considered hereafter:

1. CBT indicates the *Complete Bright Total* sample, which includes the stars with $B < 18.6$ measured over the total area AI + AII + AIII, using the short exposure plates;

2. CBA includes only the stars listed in CBT which lie within the Annulus AI (with radius from 3.5′ to 6′);

3. FA lists all the stars measured in AI and fainter than $B = 18.6$, measured on the deep exposure plates. Stars included in the sample FA have then been divided into two groups according to the degree of photometric internal errors associated to magnitudes and colours. The first group **FA1** is thus formed by all the stars whose internal photometric errors are $\sigma_B < 0.09$ mag and $\sigma_V < 0.12$ mag. They only were used to determine the mean MS ridge line. The second group **FA2** will actually be considered only in the treatments related to star counts.

Table 3 reports the number of stars measured in these samples for each individual branch. The values of V, $B-V$, X, and Y of the 1049 stars included in CBT (excluding the 96 known variables) are listed in Table 4 (published in electronic form). An "F" preceding the identification number marks field stars as identified by Cudworth (1979). Table 5 reports the cross-identifications with Sandage (1953,1970). Magnitudes, colours, and positions of the remaining 9491 stars are then reported in Table 6 (published in electronic form), and are available from the CDS at Strasbourg upon request. Individual stars specifically discussed in the text have been identified in the maps presented in Fig. 5a–d.

2.3. Photometric errors

2.3.1. Plate errors

The main problem encountered in the reductions was due to the variation of the PSF with magnitude and, in particular, position in the plate. Since most of the exposures were taken with the cluster slightly off-centered, the PSF variations do not show a regular trend with increasing radial distance from the centre of the cluster. Hence, no simple radial corrections could be applied. The use of a *local* PSF, in principle available in ROMAFOT, would have been prohibitively time-consuming due to the huge number of measured stars. The only feasible procedure was then

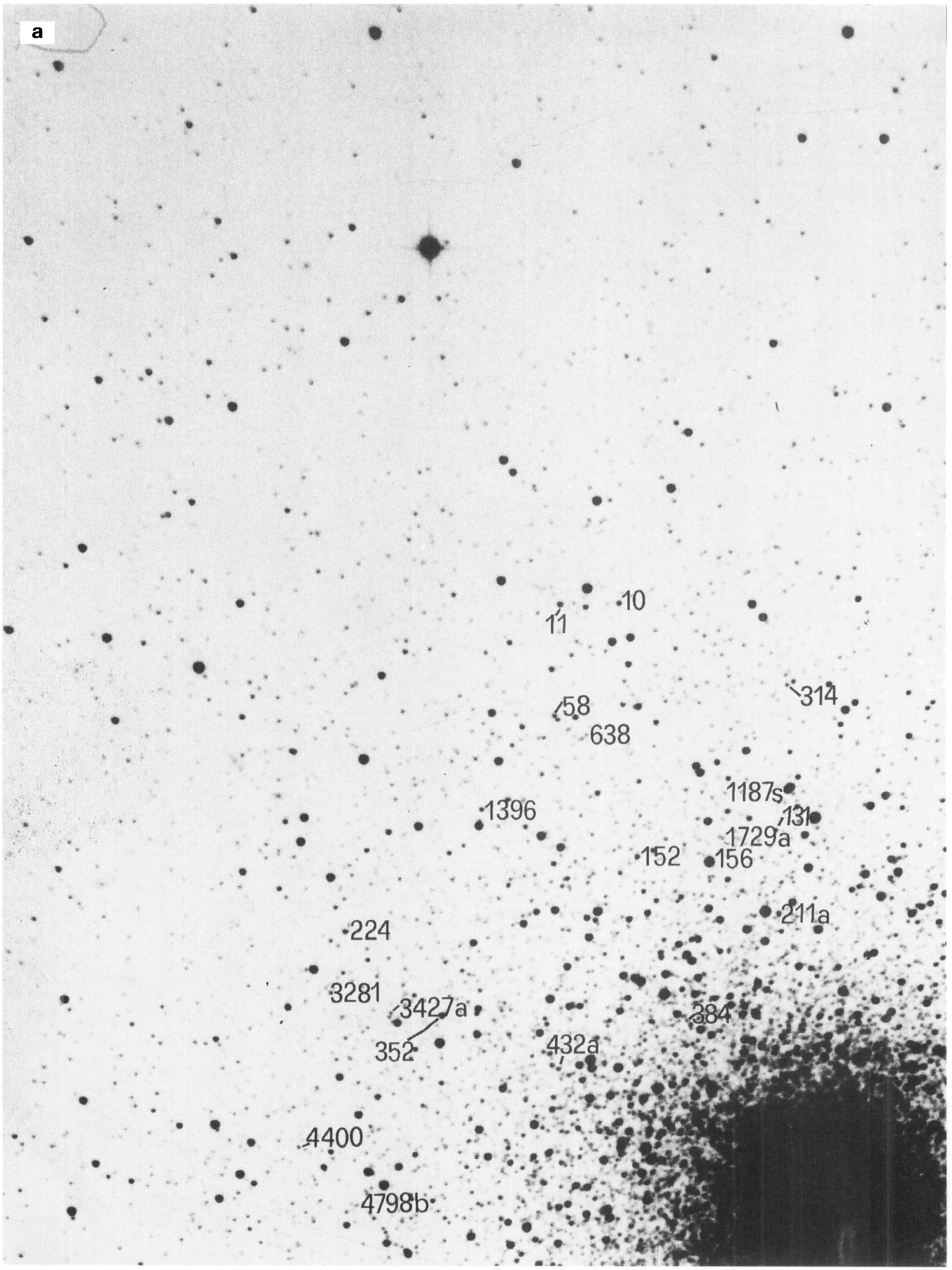

Fig. 5a–d. Maps reporting the identifications of the "special stars" discussed in the text (BSS, EHB, HEHB, ERHB, etc.) (Sects. s 3.3 and 4.2)

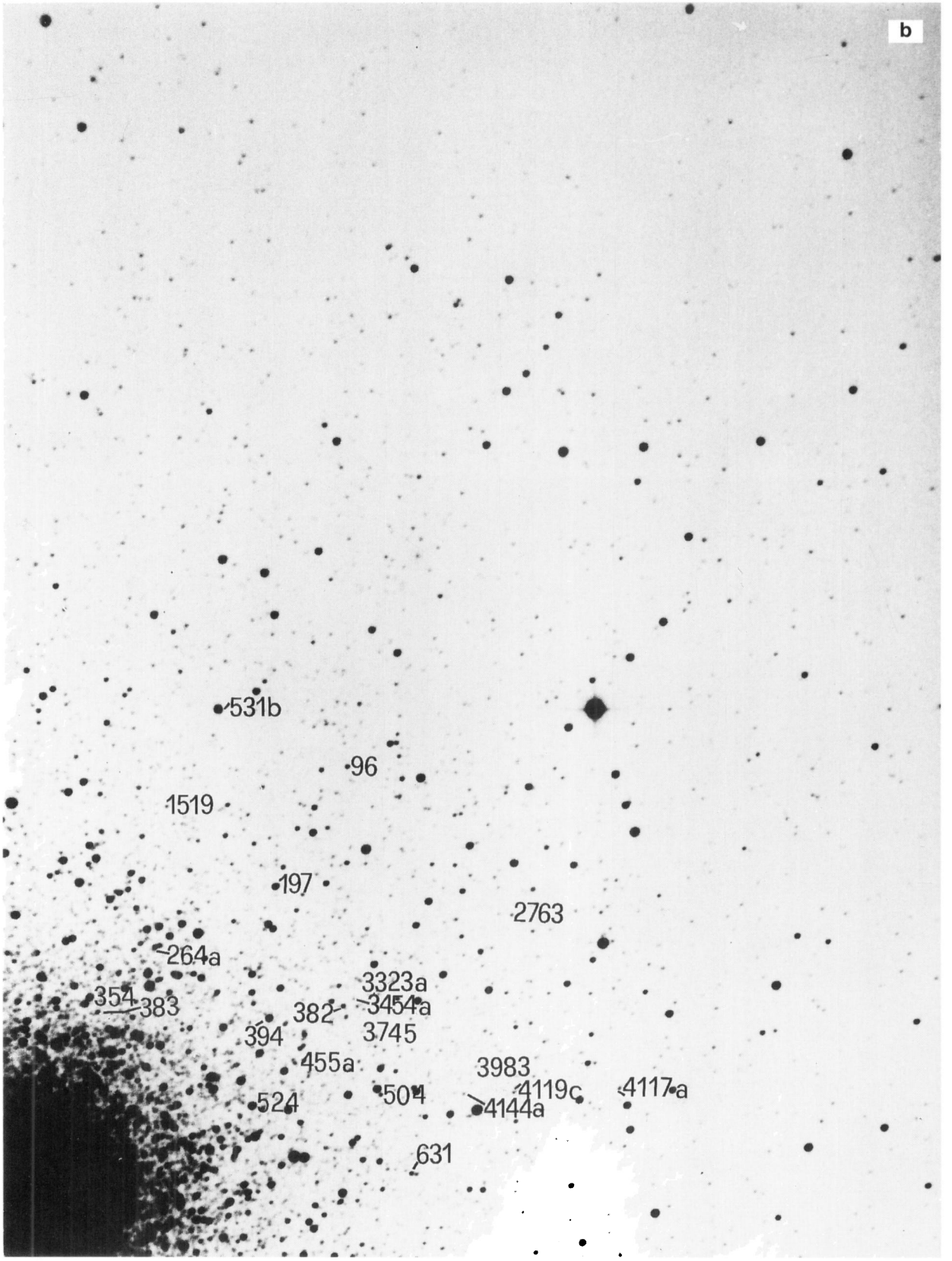

Fig. 5. (continued)

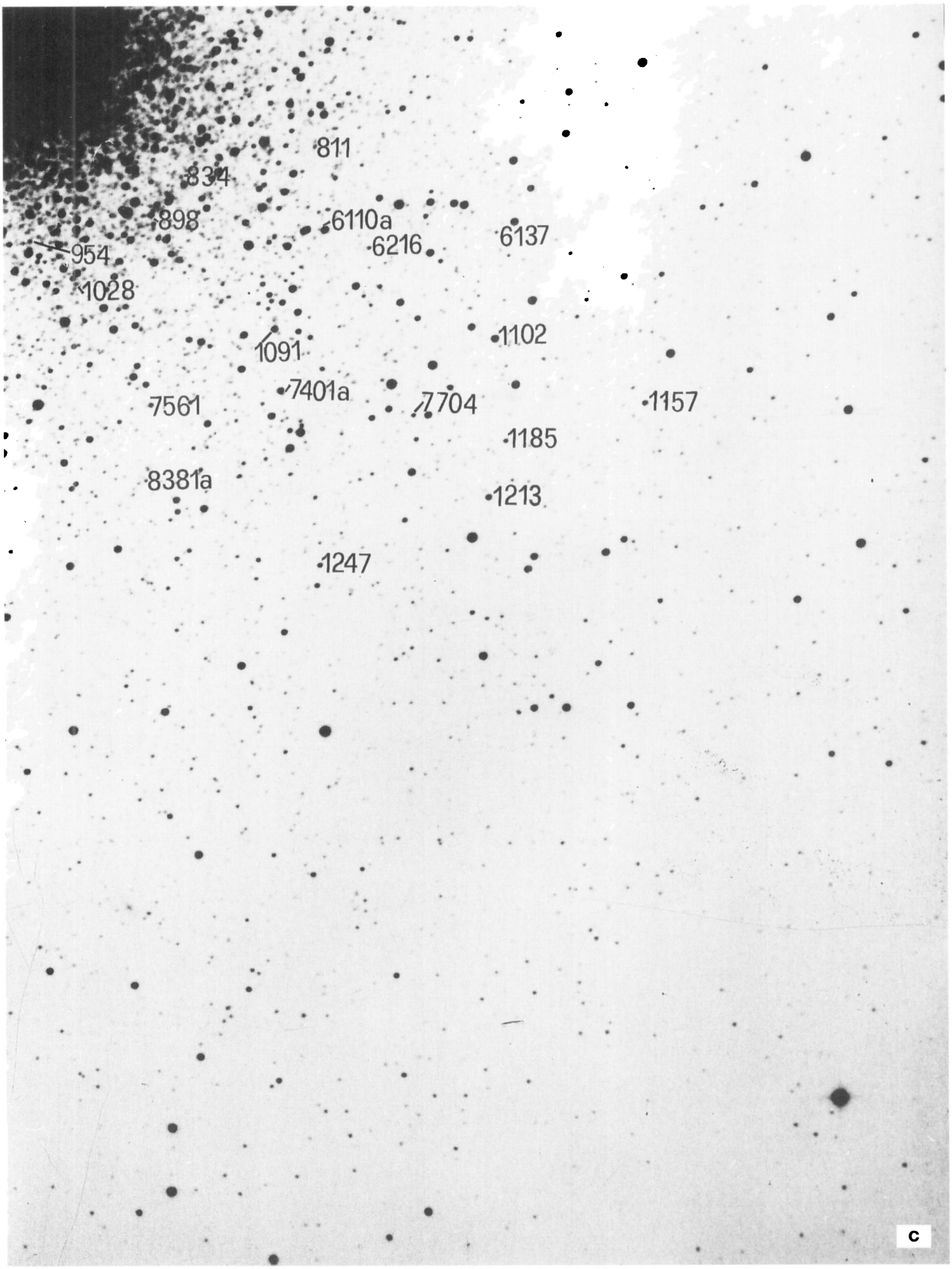

Fig. 5. (continued)

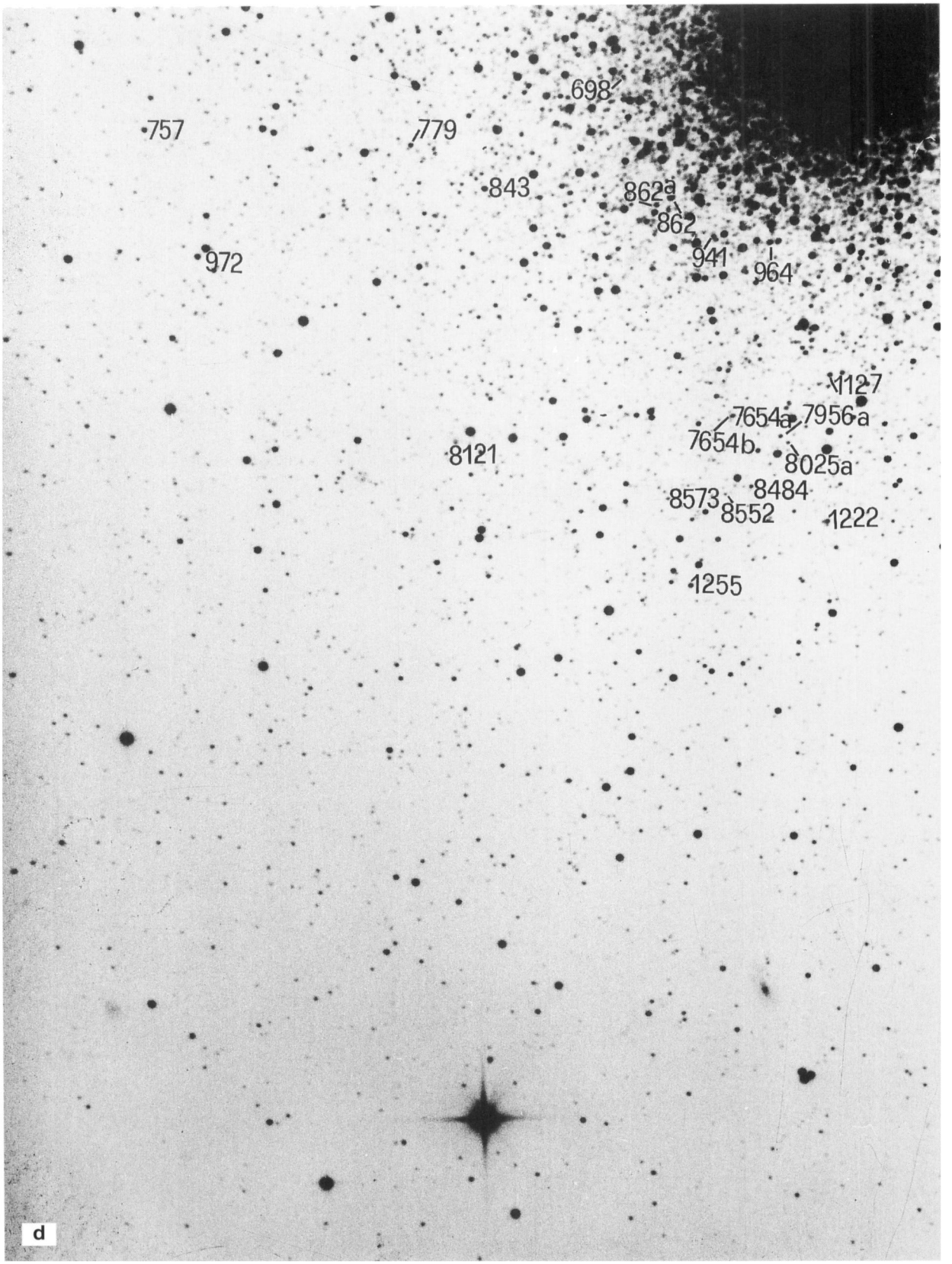

Fig. 5. (continued)

Table 2. Photoelectric standards for B V calibrations

This paper			Sandage 1970		
Star	V	$(B-V)$	Star	V	$(B-V)$
Bright sample					
78	15.73	0.09	I-III-14	15.76	0.09
39	15.72	0.08	I-II-12	15.71	0.08
96	17.47	0.10	I-III-36	17.45	0.26
20	15.64	0.15	I-II-13	15.76	0.09
52	15.58	0.45	I-II-15	15.61	0.45
54	15.67	0.13	I-II-33	15.57	0.14
109	15.60	0.15	I-II-45	15.64	0.12
156	15.03	-0.41	I-II-57	14.94	-0.30
10	17.77	0.12	II-II-29	17.80	0.26
5	14.13	0.89	I-II-18	14.09	0.94
84	15.97	-0.02	I-I-27	16.14	-0.02
125	15.82	0.01	I-I-30	15.82	0.01
268	12.74	1.41	I-III-28	12.81	1.37
526	15.41	0.45	I-III-19	15.46	0.42
542	15.49	0.42	I-III-51	15.46	0.50
445	16.27	-0.06	I-I-56	16.28	-0.07
523	15.71	0.14	I-I-51	15.82	0.07
589	16.30	-0.09	I-I-47	16.37	-0.10
543	15.67	0.45	I-I-40	15.68	0.39
628	15.65	0.35	I-I-42	15.58	0.44
1241	15.99	-0.01	I-IV-18	15.73	0.12
1280	15.72	0.16	235	15.76	0.08
1299	12.80	1.45	297	12.89	1.42
950	15.82	0.02	I-VI-26	15.76	0.01
1015	15.94	0.00	I-VI-48	15.90	0.02
1142	12.88	1.43	1397	12.65	1.56
1232	15.68	0.80	I-VI-14	15.68	0.72
352	17.01	-0.23	I-I-58	16.94	-0.10
7704	17.81	0.09	I-IV-34	17.74	0.13
1231	14.02	0.65	237	14.09	0.65
–	18.06	0.66	III-II-181	18.03	0.68
518	15.70	0.08	I-III-22	15.62	0.12
11	17.30	0.20	I-II-21	17.23	0.31
Faint sample (for plate transfer)					
–	15.65	0.51	III-9	15.61	0.48
–	19.72	0.47	F24	19.71	0.41
–	19.92	0.38	F35	19.90	0.44
–	20.18	0.43	F34	20.23	0.47
–	20.70	0.63	F25	20.74	0.54
–	20.73	0.54	F28	20.71	0.64
–	18.50	0.51	F2	18.50	0.54
–	19.11	0.34	F6	19.02	0.41
–	21.09	0.65	F23	21.05	0.65
–	15.68	0.43	II-11	15.68	0.42
–	16.81	0.65	II-9	16.74	0.71
–	15.55	0.39	II-15	15.61	0.45
–	17.71	0.64	F1	17.83	0.68
–	20.35	0.48	F10	20.43	0.49
–	16.04	0.64	F	16.02	0.56
–	19.74	0.42	F7	19.66	0.40
–	18.40	0.79	F3	18.44	0.73

Table 3. Number of stars in each individual branch from different samples

	CBT[a]	CBA[a]	FA		CBA+FA
			FA1	FA2	
MS	–	–	6033	2301	8334
SGB	–	–	905	153	1058
RGB	860	288	54	–	342
HB	223 (90)	80 (31)	–	–	80
AGB	39 (6)	10 (2)	–	–	10
HPAGB	3	2	–	–	2
BS	20	8	33	12	53
Total	1145 (96)	388 (33)			9879

[a] Variables

to use the same PSF allover the scanned areas, map the residuals in magnitude and colour taken in small sub-areas over the whole field with respect to the mean ridge line of the sequences, and apply corrections to the individual magnitudes according to the residuals.

Figure 6a,b shows an example of the correcting procedure consisting in the following steps:

(i) derive the mean ridge lines in the instrumental CMD;

(ii) compute for each star the colour residual $\delta(B-V)$ with respect to the adopted ridge line;

(iii) plot the residuals in the X, Y-plane (see Fig. 6a, *white* $\delta(B-V) < -0.05$ mag, *grey* $-0.05 < \delta(B-V) < 0.05$, *black* $\delta(B-V) > 0.05$);

(iv) assuming that no intrinsic differences exist in the position of the mean ridge line of the sequences in different areas of the cluster, we corrected all the i-magnitudes and colours via an iterative procedure based on an experimental *correction-map* until the mean of the residuals turned out to be zero over any sub-area of about $30'' \times 30''$ and over the total field.

Figures 6a and 6b present the map of the colour residuals for all the stars in the FA1 sample before and after correction respectively. This procedure is somewhat arbitrary because of the implicit assumption that there is no significant difference in the intrinsic characteristics of the cluster mean loci at different positions within the cluster. However, differential or patchy reddening, which might produce such differences, seems unlikely in this high-latitude low-reddening cluster, and we cannot think of any physical reason to expect significant intrinsic shifts of the mean ridge lines.

2.3.2. Photometric accuracy

As well known, the total photometric error results from the combination of at least three contributions:

(a) the intrinsic error in the photoelectric standards;

(b) the measuring error in each plate and in the average (internal error);

(c) the errors introduced by the transformations from the instrumental to the Standard System.

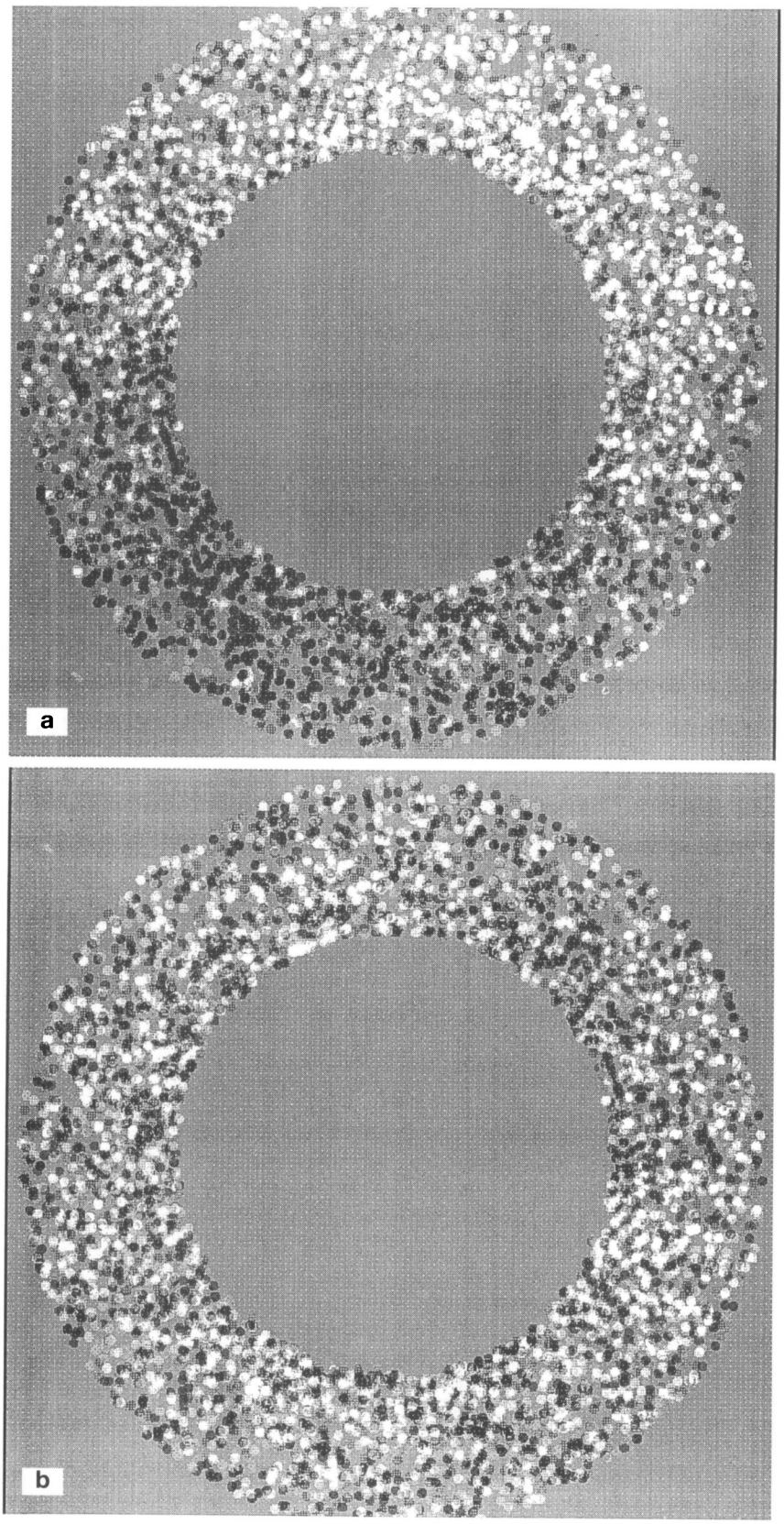

Fig. 6a and b. Results of the procedure used for plate error correction. Map of the residuals in colour (individual value - ridge line): **a** before correction, **b** after running the iterative method described in Sect. 2.3.1

Table 5. Stars in common with Sandage (1953) series I

Sandage	This paper	Sandage	This paper	Sandage	This paper	Sandage	This paper
I-I-7	19	I-I-93	422	I-III-15	129	I-III-86	308
I-I-17	574	I-I-94	448	I-III-18	503	I-III-87	524
I-I-21	31	I-I-96	512	I-III-19	526	I-IV-1	1292
I-I-27	84	I-I-97	529	I-III-20	572	I-IV-2	1285
I-I-29	126	I-I-98	491	I-III-21	645	I-IV-15	1295
I-I-30	125	I-I-100	570	I-III-22	518	I-IV-17	1244
I-I-31	142	I-I-102	569	I-III-23	462	I-IV-18	1241
I-I-32	117	I-I-103	582	I-III-25	343	I-IV-19	1236
I-I-34	266	I-I-104	615	I-III-26	291	I-IV-21	1022
I-I-36	333	I-I-105	624	I-III-28	268	I-IV-27	687
I-I-38	511	I-I-106	635	I-III-29	279	I-IV-28	725
I-I-39	509	I-I-107	600	I-III-30	182	I-IV-29	777
I-I-40	543	I-I-108	578	I-III-32	158	I-IV-30	921
I-I-41	611	I-I-109	552	I-III-33	103	I-IV-31	1025
I-I-42	628	I-II-12	2	I-III-34	105	I-IV-32	1102
I-I-43	556	I-II-13	20	I-III-35	85a	I-IV-33	1165
I-I-44	588	I-II-14	46	I-III-36	96	I-IV-35	1184
I-I-46	617	I-II-15	52	I-III-38	137	I-IV-36	1160
I-I-47	589	I-II-18	5	I-III-39	145	I-IV-37	1168
I-I-48	563	I-II-21	11	I-III-41	174	I-IV-38	1201
I-I-49	634	I-II-22	35	I-III-42	180	I-IV-39	1221
I-I-50	592	I-II-24	36	I-III-43	197	I-IV-40	1213
I-I-51	523	I-II-26	59	I-III-44	240	I-IV-41	1211
I-I-52	461	I-II-28	41	I-III-45	240a	I-IV-42	1188
I-I-53	451	I-II-32	48	I-III-47	377	I-IV-43	1175
I-I-54	470	I-II-33	54	I-III-49	340	I-IV-44	1164
I-I-55	498	I-II-34	63	I-III-50	371	I-IV-45	1125a
I-I-56	445	I-II-35	74	I-III-51	542	I-IV-46	1094
I-I-57	411	I-II-36	113	I-III-52	545	I-IV-47	1091
I-I-58	352	I-II-37	107	I-III-53	466	I-IV-48	1096
I-I-59	309	I-II-38	147	I-III-54	469	I-IV-49	1107
I-I-60	388	I-II-39	146	I-III-55	505	I-IV-50	1103
I-I-62	236	I-II-40	138	I-III-56	495	I-IV-51	1100
I-I-63	220	I-II-42	166	I-III-57	621	I-IV-52	1067
I-I-64	203	I-II-43	185	I-III-58	616	I-IV-53	1047
I-I-65	202	I-II-44	188	I-III-59	649	I-IV-55	1029
I-I-66	216	I-II-45	109	I-III-60	652	I-IV-56	1038
I-I-67	230	I-II-47	134	I-III-61	656	I-IV-59	1034
I-I-69	210	I-II-48	110	I-III-62	631a	I-IV-60	1052
I-I-70	157	I-II-50	93	I-III-63	657	I-IV-61	1073
I-I-71	139	I-II-51	80	I-III-64	614	I-IV-63	932
I-I-72	132	I-II-52	86	I-III-65	636a	I-IV-64	869
I-I-73	127	I-II-53	88	I-III-66	548	I-IV-65	913
I-I-75	281	I-II-54	90	I-III-67	580a	I-IV-66	880
I-I-76	312	I-II-56	100	I-III-68	580	I-IV-67	885
I-I-77	356	I-II-57	156	I-III-69	528	I-IV-68	893
I-I-78	384	I-II-58	172	I-III-70	520	I-IV-69	747
I-I-79	375	I-II-59	193	I-III-71	468	I-IV-70	749
I-I-80	283	I-II-61	190	I-III-72	444	I-IV-71	753
I-I-81	287a	I-II-62	228	I-III-73	409	I-IV-72	751
I-I-82	325	I-II-63	201	I-III-74	394	I-IV-73	756
I-I-83	347	I-II-64	256	I-III-75	344	I-IV-74	736
I-I-84	337	I-II-65	273	I-III-76	348	I-IV-75	701

Table 5. (continued)

Sandage	This paper	Sandage	This paper	Sandage	This paper	Sandage	This paper
I-I-85	336	I-II-66	244	I-III-77	247	I-IV-76	697
I-I-86	434	I-II-67	254	I-III-78	284	I-IV-77	786
I-I-87	424	I-II-68	304	I-III-79	237	I-IV-78	831
I-I-88	438	I-III-6	26	I-III-80	332	I-IV-79	858
I-I-89	449	I-III-12	39	I-III-81	431	I-IV-80	890
I-I-91	472	I-III-13	47	I-III-84	641	I-IV-81	917
I-I-92	477	I-III-14	78	I-III-85	418	I-IV-84	982
I-IV-85	806	I-V-39	1130	I-V-77	1017	I-VI-52	683
I-IV-86	953	I-V-40	1119	I-V-78	973	I-VI-54	843
I-IV-87	865	I-V-41	1192	I-V-79	937	I-VI-55	919
I-IV-88	845	I-V-43	1195	I-V-80	942	I-VI-56	961
I-IV-89	789	I-V-44	1190	I-V-81	966	I-VI-57	978
I-IV-90	770	I-V-45	1204	I-V-82	947	I-VI-58	1032
I-IV-91	776	I-V-46	1217	I-V-83	925	I-VI-59	1031
I-IV-92	760a	I-V-48	1245	I-VI-16	1183	I-VI-60	981
I-IV-94	837	I-V-50	1248	I-VI-17	1084	I-VI-61	983
I-IV-95	708	I-V-51	1215	I-VI-21	724	I-VI-62	930
I-IV-98	952	I-V-52	1210	I-VI-22	759	I-VI-63	820
I-IV-99	1099	I-V-53	1205	I-VI-24	764	I-VI-64	819
I-IV-100	1092	I-V-54	1161	I-VI-25	881	I-VI-65	841
I-IV-101	1131	I-V-55	1170	I-VI-26	950	I-VI-66	853
I-IV-102	997	I-V-56	1140	I-VI-28	992	I-VI-67	970
I-V-15	1301	I-V-57	1120	I-VI-29	1104	I-VI-68	910
I-V-16	1283	I-V-58	1122	I-VI-30	1177	I-VI-69	810
I-V-17	1276	I-V-59	1133	I-VI-31	1223	I-VI-70	797
I-V-18	1259	I-V-60	1068	I-VI-34	1228	I-VI-71	758
I-V-20	1289	I-V-61	1060	I-VI-36	1249	I-VI-72	769
I-V-23	1281	I-V-62	1127	I-VI-38	1225	I-VI-73	733
I-V-24	1293	I-V-64	1124	I-VI-39	1176	I-VI-74	734
I-V-27	1242	I-V-65	1118	I-VI-40	1163	I-VI-75	689a
I-V-28	1239	I-V-66	1106	I-VI-41	1155	I-VI-77	686
I-V-29	1243	I-V-67	1111	I-VI-42	1141	I-VI-78	694
I-V-30	1206a	I-V-68	1085	I-VI-43	1083	I-VI-79	655
I-V-31	1206	I-V-69	1080	I-VI-44	1072	I-VI-80	663
I-V-32	1197	I-V-70	1087	I-VI-45	1048	I-VI-81	688
I-V-33	1182	I-V-71	1016	I-VI-46	1062	I-VI-82	726
I-V-34	1173	I-V-72	993	I-VI-47	995	I-VI-83	750
I-V-35	1166	I-V-73	1010	I-VI-48	1015	I-VI-84	772
I-V-36	1169	I-V-74	988	I-VI-49	798	I-VI-85	795
I-V-37	7561	I-V-75	1014	I-VI-50	668	I-VI-86	809
I-V-38	1148	I-V-76	1019	I-VI-51	744		

The comparison between photographic and photoelectric data is considered usually to be a good estimate of the total error involved if two conditions are verified:

(i) the photoelectric data cover an appropriate magnitude and colour range;

(ii) the stars used for the calibrations and the program stars are treated in the same way throughout the whole procedure.

Errors in the photoelectric standards depend on magnitude, colour, and position of the standard stars within the cluster. Our *conservative* estimate of the photometric uncertainties affecting the stars listed in Tables I and II of Sandage (1970) adopted here as calibrators is ± 0.05 mag, including also a possible uncertainty of the zero-point. Since we did not carry out at this stage any independent observations of standard stars, the global absolute accuracy of the measures presented here cannot be better than such a value.

The internal errors can be easily determined from the rms plate-to-plate scatter of the magnitudes and colours of individual stars. Figure 7a–d show these rms-values as a function of magnitude. All the errors increase with increasing the magnitude, but they remain sufficently low even at the faint end, as we stopped our search just about half a magnitude brighter than the instrumental detection limit on each plate in order to avoid measuring of a huge number of stars yielding anyway too uncertain

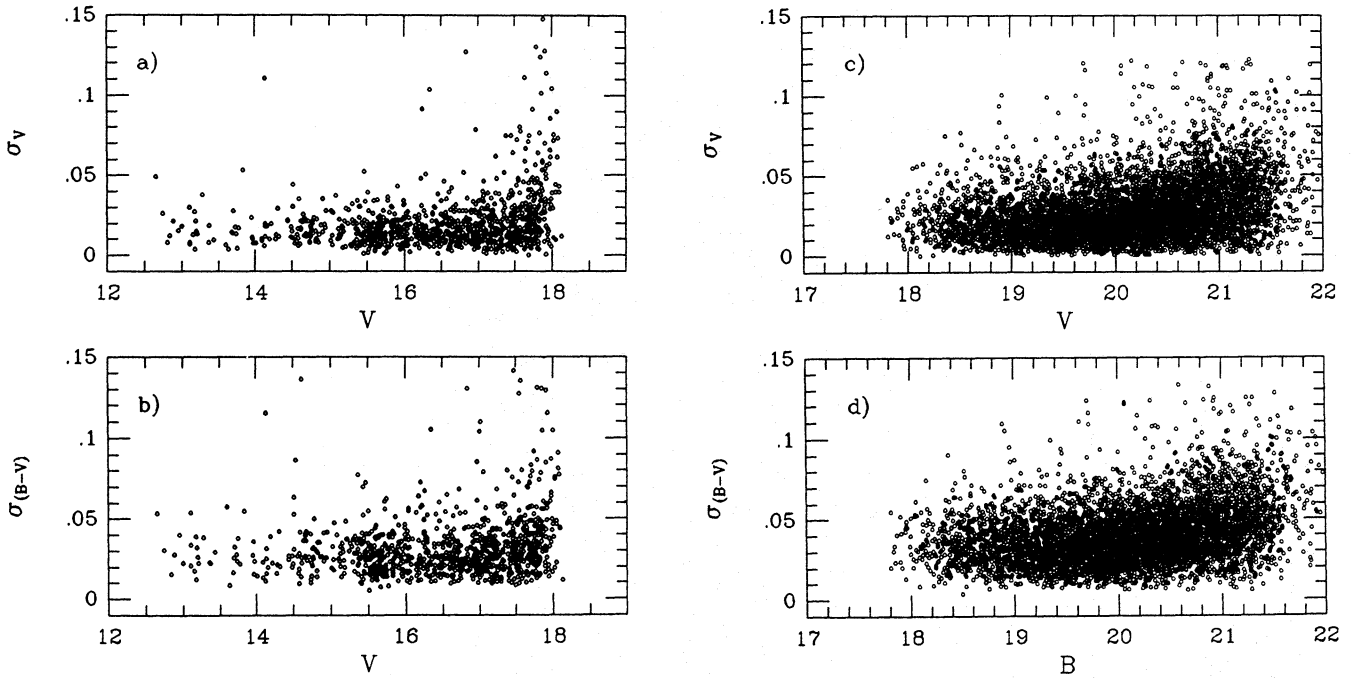

Fig. 7a–d. Internal photometric errors of the photographic photometry. The rms values of the plate-to-plate scatter, expressed in magnitudes, for the bright and faint samples are plotted versus the mean magnitudes (Sect. 2.3.2)

magnitudes. Note that, since different samples come from different plates obtained with highly different exposure times, the bright objects of the faint sample (Fig. 7c,d) have smaller internal errors than the faint objects of the bright sample (Fig. 7a,b), even if they may have the same magnitude. The large rms errors found for some objects are usually due to problems related to a difficult fitting of blended images. A few of them could also result from intrinsic variability of the measured star, but the number of plates we measured is too small to get any firm hint on possible variability.

Finally, as can be seen from Figs. 2, 3, and 4 there are small intervals (over the whole magnitude range covered) where only a few photoelectric standards were available and also the coverage in colour is not fully adequate. Therefore the presence of small ($\sim 0.02 - 0.03$ mag) residual systematic errors in magnitude and colours even with respect to the adopted Sandage (1970) reference system cannot be totally excluded, while we are confident that no residual systematic trend is present with the background.

Because of the better reduction technique and the accurate treatment of the background, we estimate that the photometric acuracy of the present data is better than in Sandage (1953) for the stars in similar crowding conditions.

A new, totally independent revision of the whole photometry in M 3, which we carried out using recent CCD data, is in progress and will be reported in a forthcoming paper (Ferraro et al. 1994).

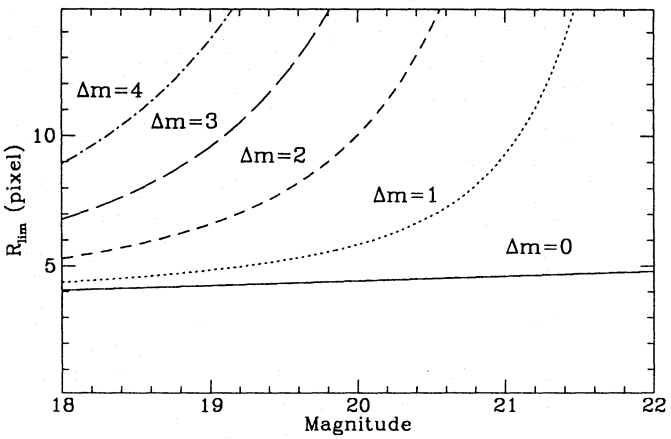

Fig. 8. Plot of the *minimum* distance at which two stars of magnitude m and $m + dm$ can still be detected as single objects in the present photometry. The curves were computed using Eq. (4) (Sect. 2.4)

2.4. Completeness

Completeness is a primary requirement to be achieved when trying to dig into questions other than the simple definition of the stellar main loci in the CMD, and is one of the major goals we have reached with the present work with respect to Sandage (1953). However, it is *unrealistic* to expect the detection of *all* the cluster stars from ground-based observations, whatever is the procedure adopted for the reductions. Therefore, the problem of completeness can be reduced to the problem of a *reliable* estimate of the efficiency of the algorithm used in the detections.

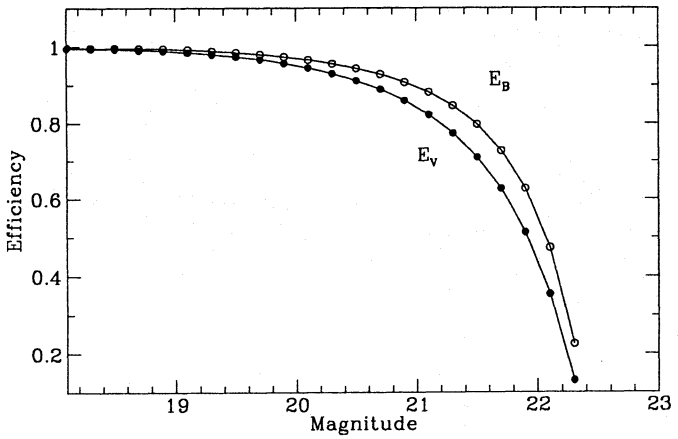

Fig. 9. Efficiency in the star detection and completeness curves derived from the procedure described at Sect. 2.4

To estimate the degree of completeness we presently use the standard procedure based on "adding-and-recovering artificial stars" from the frames, which yields "direct" measures of incompleteness. However, the photometric data presented here were obtained in 1984, when this facility was still not available in ROMAFOT. It would thus be necessary to re-reduce all the plates to apply the procedure directly to each of them. Therefore, in order to estimate the degree of completeness without spending a huge amount of time in redoing the entire reduction work, we carried out some tests in two properly chosen fields adopting the following semi-empirical approach.

Let $N_{\rm obs}$ be the number of stars detected down to a given magnitude level m^* on a frame covering a total area $A_{\rm tot}$. Since each star has a *finite* area σ (which can be computed from the PSF) we expect that a fraction f of the frame is *obscured* by the $N_{\rm obs}$ detected objects:

$$f_m = \frac{\sum^{N_{\rm obs}} \sigma_m}{A_{\rm tot}} = \frac{A_*}{A_{\rm tot}} \leq 1 \qquad (1)$$

where A_* is the total obscured area on the frame.

Clearly the fraction f is a function of the magnitude m as $N_{\rm obs} = N_{\rm obs}(m)$ is the cumulative observed luminosity function of the cluster and $\sigma = \sigma(m)$ varies, increasing with increasing luminosity of the stars. A number δN_{m^*} of undetected stars brighter than magnitude m are therefore embedded in the obscured area, and the detection efficiency E_m is:

$$E_m = \frac{N_{\rm obs}}{(N_{\rm obs} + \delta N)}\Big|_{m \leq m} = 1 - f_m \qquad (2)$$

The correction δN to be added to the observed cumulative luminosity function $N_{\rm obs}(m)$ is then:

$$\frac{\delta N}{N_{\rm obs}}\Big|_{m \leq m} = \frac{1-E}{E} = \frac{f}{1-f} = \frac{A}{A_{\rm b}} \qquad (3)$$

where $A_{\rm b}$ is the *blank* area on the frame (i.e. $A_{\rm b} = A_{\rm tot} - A$).

Crucial in this procedure is to evaluate the *effective area* σ_m of each detected star. This quantity depends on magnitude, seeing, plate quality and (especially) on the actual *efficiency* of the algorithm of detection. The more efficient is the detection procedure, the lower is σ at a given magnitude for a given PSF.

ROMAFOT carefully deals with the problem of blended images, being easily able to recognize objects "hidden" in composite PSFs. In particular, we have quantitatively evaluated its actual efficiency here through an appropriate number of tests involving the analysis of a couple of images of single stars at different *relative* distances on the plates and with different magnitudes. The two stars (extracted from the original frames) were *artificially* shifted to become closer and closer until the algorithm recognized them as "one merged object". From these tests a useful analytical relation was derived, that evaluates the *minimum* distance – $R_{\rm lim}$ – at which two stars of magnitudes m and $m + \Delta m$ can still be detected as single objects:

$$R_{\rm lim} = \left[\frac{38}{(23-m)^3 + 0.1}\right](\Delta m)^2 + 0.183\ m + 0.77 \qquad (4)$$

Here $R_{\rm lim}$ is given in units of pixels, the scale being 1 px = 0.223 arcsec. Equation (4) is displayed in a graphic form also in Fig. 8. From this equation one can appreciate the efficiency of the algorithm: for instance two stars of the same magnitude can still be picked up as two "separate" objects at a relative distance of $\sim$ 4–5 pixels (0.8–1.0 arcsec).

Using this expression for $R_{\rm lim}$, one can then derive:

$$\sigma_{(m,\Delta m)} = \pi R^2_{lim\ (m,\Delta m)} \qquad (5)$$

and the correction for incompleteness can then proceed through the following steps:

(1) The stellar counts in each bin (0.2 mag wide) of magnitude m^* have been corrected by a fraction derived from Eq. (3) after having evaluated f by means of Eq. (1). In Eq. (1) the cross sections σ_m [as defined by Eq. (5)] have been summed up over all the *detected* stars with $m \leq m^*$.

(2) The detection efficiency E_{m^*} has been calculated via Eq. (2).

(3) Both the B and V cumulative observed LF have been progressively scanned down to fainter and fainter magnitudes.

The resulting functions E_V and E_B are shown in Fig. 9 where one can see that the detection efficiency E is better than 90% until approximately $V \leq 20.6$ or $B \leq 21.0$, while three stars over four have been still detected and measured at $V = 21.4$ or $B = 21.7$.

Finally, Table 7 presents the results of the completeness test using the above described procedure and the technique of the "artificial" stars. One can see that the two procedures agree within a few percent at least until the degree of completeness is larger than about 85%. Some significant discrepancies appear only very close to the plate limit. On the other hand, we have already stressed that the "search phase" has generally not been pushed to the plate limit just to avoid the high incidence of incompleteness and large photometric errors.

3. Colour-magnitude diagram

The CMD of all the measured stars in M 3 excluding those belonging to the FA2 sample (less accurate photometry), is pre-

Table 7. Results of the completeness tests

V	N_{in}	N_{out}	E_{test}	$E_{eq.}$
18.90	60	60	1.000	0.988
19.10	60	60	1.000	0.984
19.30	60	58	0.967	0.979
19.50	60	60	1.000	0.973
19.70	60	59	0.983	0.966
19.90	60	57	0.950	0.956
20.10	60	53	0.900	0.944
20.30	60	57	0.950	0.930
20.50	60	52	0.867	0.911
20.70	60	58	0.967	0.889
20.90	60	51	0.850	0.859
21.10	60	45	0.750	0.822
21.30	60	52	0.867	0.774
21.50	60	39	0.650	0.710
21.70	60	42	0.700	0.627

N_{in} : number of inserted artificial stars
N_{out} : number of detected artificial stars
E_{test} : N_{out}/N_{in}
$E_{eq.}$: from Eq. (2)

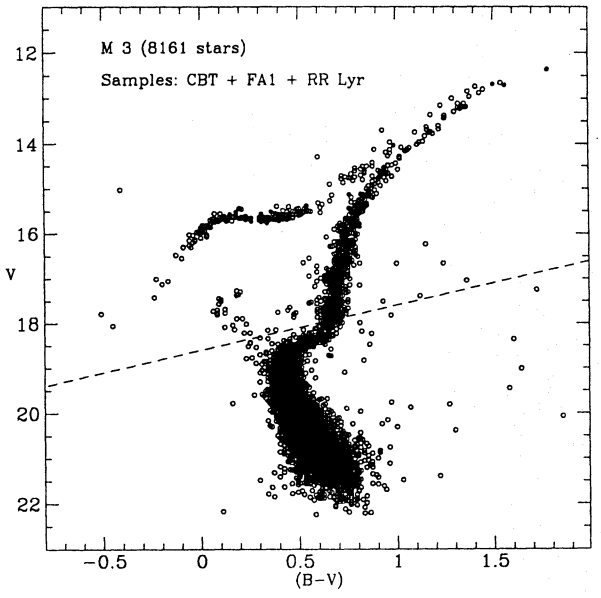

Fig. 10. Colour-magnitude diagram of the CBT + FA1 + RR Lyr samples. CBT = *Complete Bright Total* sample, which includes the stars with $B < 18.6$ (dotted line) measured over the total area AI+AII+AIII. FA1 = *Faint A1* sample, formed by all the stars measured within the annulus with $3.5' < r < 6.0'$ and with internal photometric errors $\sigma_B < 0.09$ mag and $\sigma_V < 0.12$ mag. RR Lyr = RR Lyrae variables as listed in Table 10

sented in Fig. 10. The dashed line shows the separation between the bright CBT sample and the faint FA1 stars. Magnitudes and colours of 7413 stars are plotted in the diagram and the apparent "wideness" of the MS is mainly an optical effect of projecting on the paper the wings of a huge distribution of stars whose FWHM is instead remarkably narrow (see Sect. 3.1.2). Note that also the RR Lyrae variables present in the measured area have been inserted in the CMD by adopting proper mean magnitudes (see Sect. 3.3). As expected, they fill the typical HB gap for the instability strip location.

The CMD resembles very closely those already published by previous studies of the same cluster (Sandage 1953, 1970; Kadla & Gerashchenko 1982; Sandage & Katem 1982; Aurière & Cordoni 1983; Paez et al. 1990) and the existence of a sizeable population of BSS is confirmed. The main general features that may be noticed are:

(1) All the main branches are well-defined and clearly separable (including RGB and AGB).

(2) The MS turnoff is at $V_{TO} = 19.17 \pm 0.07$ (where the measure has been made by making proper histograms in colour and various fits of the overall turnoff region, and the error is an estimate deduced from the whole procedure).

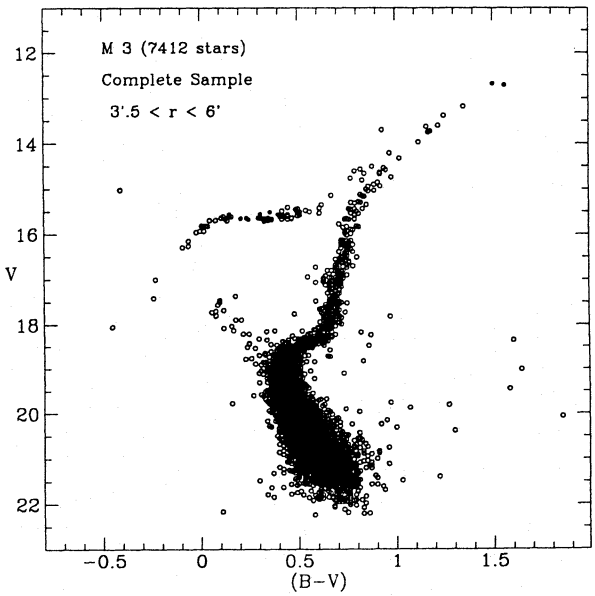

Fig. 11. Colour-magnitude diagram of the CBA + FA1 + RR Lyr samples. This diagram includes only the sub-sample of the stars plotted in Fig. 10 located within the annulus with $3.5' < r < 6.0'$. The stars included in the FA2 sample (worse photometric quality, see Sect. 2.2) have to be added in order to obtain the Total Complete Sample over the considered annulus (see Table 3)

(3) The BSS population simulates an extension of the MS and the brightest candidate is almost two magnitudes brighter than turnoff stars. There are some groups of stars located in the region of the CMD bounded by the the BSS sequence and the SGB which are worth of specific attention (see Sect. 4.3).

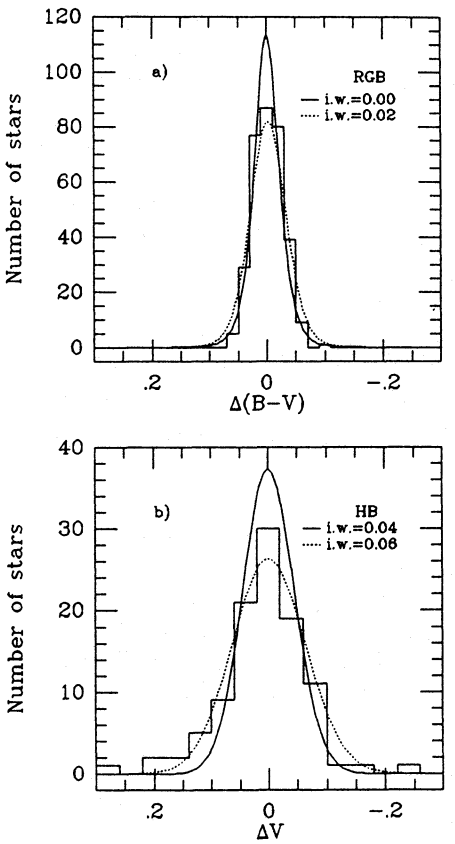

Fig. 12a and b. Determination of the intrinsic width of the RGB and HB (Sect. 3.1) **a** Distribution of the colour-residuals for the RGB over the range $15.0 < V < 17.0$ and $0.68 < B - V < 1.00$ (327 stars). **b** Distribution of the magnitude-residuals for HB stars with $15.2 < V < 16.2$ and $0.00 < B - V < 0.57$ (103 stars)

(4) The apparent decrease of the population of the SGB with respect to the RGB is a spurious effect and is entirely due to the different areas covered by the bright and the faint samples plotted in Fig. 10 and by the already discussed difference in the exposure levels of the corresponding sets of plates. It disappears when plotting only the stars listed in the complete sample CBA measured over area AII. In Fig. 11 there is just a weak photometric widening of the SGB at the junction between the samples coming from plates with different exposures. There is no evidence for the existence of gaps along the Main Sequence or the SGB such as those found or claimed in other clusters (NGC 288: Buonanno et al. 1984; ωCen: Da Costa & Villumsen 1981; NGC 6752: Cannon 1981, but see Buonanno et al. 1986; NGC 5897: Sarajedini 1992; Ferraro et al. 1992c).

(5) The RGB can easily be traced up to the tip and presents quite a steep slope, typical of intermediate metal poor clusters. The so-called "RGB-bump" is detectable at $V \sim 15.40 \pm 0.05$ (Fusi Pecci et al. 1990).

(6) The HB is narrow and shows the presence of four stars at the blue extreme, clearly separated by a gap from the bulge of the blue HB tail. The mean observed magnitude of the HB at the level of the instability strip is $V_{HB} = 15.63 \pm 0.05$.

(7) Although not easy in the upper part, the separation between the RGB and the AGB is feasible and also the AGB base can be reliably located at $V \sim 15$.

(8) The Post-AGB phase is surely represented in the sample by one star at least, i.e. the well known object *von Zeipel 1128* ($V = 15.03$, $B - V = -0.41$). Two other stars are even bluer, i.e. 524 ($V = 17.79$, $B - V = -0.51$) and 7561 ($V = 18.06$, $B - V = -0.45$), and might be UV-bright stars evolving in a post-AGB or a post-HB phase (see Sect. 3.3.4 for a discussion).

3.1. Normal points for the main branches and intrisic widths

3.1.1. Normal points

The absolute position of the different branches in the CMD depends on the reliability of the absolute photometric calibration, i.e. on the quality and quantity of the standards and on the knowledge of the appropriate colour equation. In particular, as it was already stressed (Buonanno et al. 1985, hereafter BCF85), often the absolute position of the very blue and red extremes of the branches have rather low confidence as they are determined by using only a few available standards of the appropriate colour. Since in the present study we have not obtained a new set of standards with respect to the previous study (Sandage 1970), any difference should be attributed to the different treatment of colour equations and background influence.

The normal points for the mean ridge line of the various branches are presented in Table 8. They have been obtained by making colour and magnitude histograms along the branches and rejecting a few stars deviating by more than 3σ from the ridge lines.

3.1.2. Intrisic widths (IW)

In this section we shall verify whether the scatter around the ridge-lines of the various branches in the CMD of Fig. 10 and 11 is entirely due to measurement errors or whether it is possible to derive some hints on the intrinsic width (IW) of these branches after appropriate deconvolution of the observed residuals and internal errors.

We recall here that, while correcting for plate errors (see Sect. 2.3.1), we have "forced" the MS ridge lines obtained in different areas of the plates to coincide, and this procedure has yielded small photometric corrections ($\sim 0.02 - 0.03$ mag) depending on the position of the star in the plates. Although this assumption could introduce systematic effects in the data if the "true" ridge line varied across the cluster, we have verified that it does not affect the distribution of the residuals around the "local" ridge line. Hence, it is still meaningful to study the distribution of the stars in colour around the mean locus.

The procedure adopted here is very similar to that described in Sandage & Katem (1983), the only difference being in our assumption that the observed histogram of the error distribution represents correctly the true probability distribution of the

Table 8. Mean ridge lines for the M 3 main branches

MS + SGB + RGB				HB		AGB	
V	$(B-V)$	V	$(B-V)$	V	$(B-V)$	V	$(B-V)$
21.60	0.690	16.80	0.708	17.80	−0.30	15.01	0.70 [a]
21.40	0.665	16.60	0.717	17.40	−0.25	14.82	0.75
21.20	0.640	16.40	0.729	17.05	−0.20	14.64	0.80
21.00	0.610	16.20	0.742	16.70	−0.15	14.45	0.85
20.80	0.585	16.00	0.755	16.45	−0.10	14.29	0.90
20.60	0.558	15.80	0.773	16.20	−0.05	14.12	0.95
20.40	0.535	15.60	0.791	15.95	0.00	13.96	1.00
20.20	0.505	15.40	0.815	15.82	0.05	13.79	1.05
20.00	0.480	15.20	0.845	15.70	0.10	13.63	1.10
19.80	0.460	15.00	0.875	15.65	0.15	13.46	1.15
19.60	0.445	14.80	0.915	15.63	0.20	13.30	1.20
19.40	0.430	14.60	0.955	15.63	0.25	13.14	1.25
19.20	0.420	14.40	1.002	15.63	0.30	12.98	1.30
19.00	0.422	14.20	1.055	15.63	0.35	12.85	1.35
18.80	0.444	14.00	1.108	15.63	0.40	12.75	1.40
18.60	0.475	13.80	1.162	15.60	0.45	12.65	1.45
18.40	0.555	13.60	1.215	15.55	0.50	12.55	1.50
18.20	0.620	13.40	1.268	15.50	0.55		
18.00	0.655	13.20	1.322	15.35	0.60		
17.80	0.665	13.00	1.375	15.20	0.65		
17.60	0.675	12.80	1.45				
17.40	0.684	12.60	1.55				
17.20	0.691	12.40	1.70				
17.00	0.698						

[a] HB ⇒ AGB junction

errors:

$$n(\Delta_j) = \sum_{i=1}^{N} \int_j \mathrm{erf}\ (\epsilon_i)$$

where $n(\Delta_j)$ is the number of stars expected in the j-th bin of the histogram of the residuals, N is the total number of stars in the sample, ϵ_i is the random internal error associated to the i-th star, and erf(ϵ_i) is the "error function".

Each ith star in the sample is represented by a Gaussian profile centered on the ridge line, having unity area and standard deviation ϵ_i. From this Gaussian it is possible to evaluate the probability of finding the actual measure of the colour of the ith star at a given distance from the ridge-line. A simple sum of these probabilities in each bin of residuals, then extended to all the stars in the considered portion of the CMD, gives the expected distribution of the residuals around the ridge-line as due only to measurement errors, properly normalized to the total number of stars included in the sample.

This "error-distribution law" (obtained in numerical form) can then be convolved with a known adopted distribution in order to build a simulated distribution of the residuals to be compared with the observed one. In this way we can have information on the IW of the various branches from the trial distribution which (after deconvolution) best reproduces the empirical distribution.

For sake of simplicity we adopt Gaussian distributions, but we shall perform simple tests to check the symmetry of the intrinsic distribution about the ridge line.

This procedure can deal only with the treatment of the random errors, and if systematic trends are introduced in the distributions for instance by crowding (i.e. unresolved blends), they cannot be disentangled from the intrinsic ones. This implies some caution before drawing any conclusions.

The procedure described above has been applied to the RGB-star colour residuals over the range $15.0 < V < 17.0$ and $0.68 < (B-V) < 1.00$ (327 stars), to the HB-star V-magnitude residuals in the region $15.2 < V < 16.2$ and $0.00 < (B-V) < 0.57$ (103 stars), and to the MS-star colour residuals over the interval $19.5 < V < 21.0$ and $0.30 < (B-V) < 1.00$ (3460 stars). The results of this analysis are shown in Figs. 12a,b and 13a,b,c,d,e. The sense of the difference in the residuals is always mean–observed.

Figure 12a shows the frequency histogram of the colour residuals of the RGB. Also represented are the distribution of the residuals obtained via simulations if the intrinsic width were $\sigma = 0.00$ mag and $\sigma = 0.02$ mag. From the inspection of this plot we can conclude that the IW of the RGB should be very close to zero and, anyway, not larger than 0.02 mag.

A similar plot is shown in Fig. 12b for the V-residuals of the HB stars. Here the conclusion is that the HB IW should be

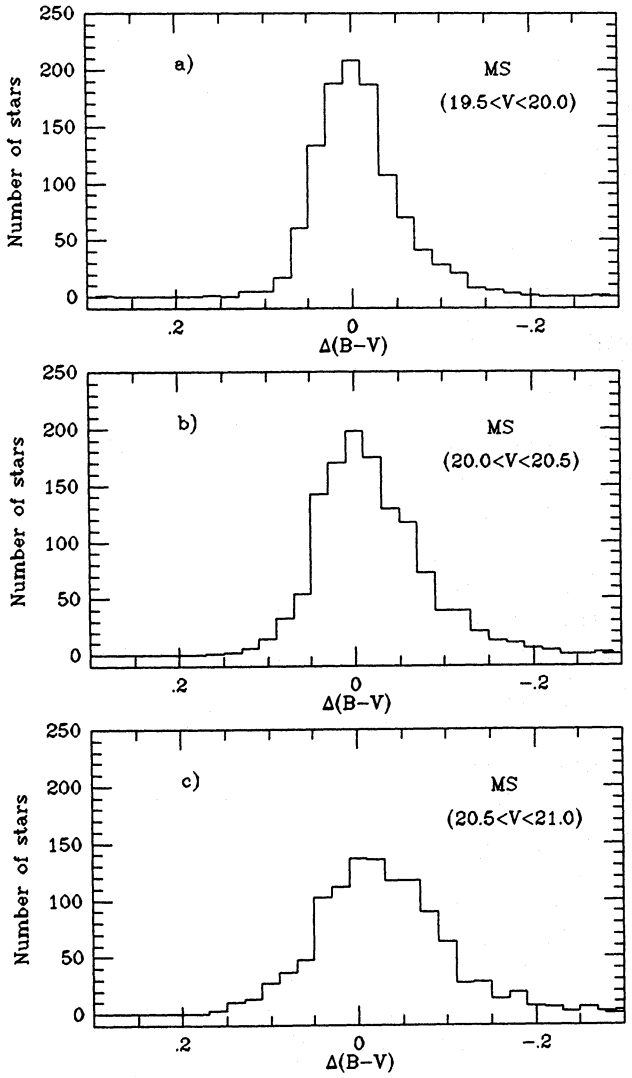

Fig. 13a–c. Histograms of the colour-residuals (ridge line – observed) with respect to the adopted MS mean ridge line in various luminosity intervals. Note the slightly enhanced wing on the red side which produces a clear skewness at any magnitude range (3460 stars in total). Though the problems involved in the data reductions suggest some caution in the interpretation of the present results, these plots may indicate the existence of a small fraction of physical or optical binaries

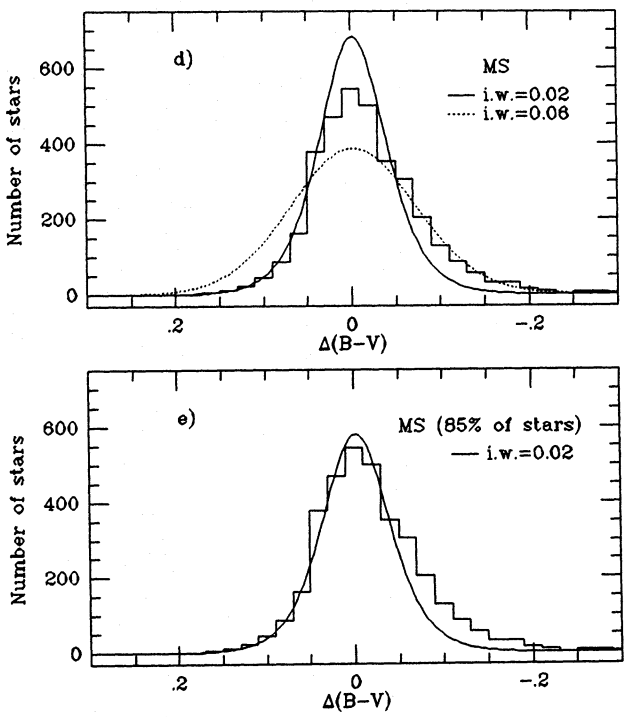

Fig. 13d and e. Distribution of the colour-residuals for the MS stars and estimate of the intrisic width of the MS (Sect. 3.1.2). The two lines in **d** report the best fitting distributions and the corresponding intrinsic widths obtained by imposing a proper matching of the blue (full line) and red (dotted line) side of the total distribution. The clear difference is due to the skewness which is further confirmed (in **e**) by the best fitting of the blue side carried out excluding 15% of the total stars having worse photometry

about 0.04 – 0.06 mag, and definitely hardly compatible with being either zero or significantly larger than 0.1 mag. The value found by Sandage (1990, hereafter S90) for the total width of the HB in M 3 was much larger (0.27 mag), but it referred to the entire spread in magnitude of the HB stars, and not to the 1σ-value of the distribution. The two figures are thus compatible. We note also that the observed distribution in Fig. 12b is somewhat "skewed" towards the luminous side, possibly due to the evolution of HB stars off the ZAHB, again compatible with S90 (see Sect. 3.3).

Turning to the MS, the distribution of colour residuals presents quite a marked "skewness" towards the red side of the ridge line. This evidence shows up clearly in the histograms presented in Fig. 13a,b,c where the stars in the MS sample have been divided into three sub-samples, and all of them show the same asymmetrical distribution. Even taking into account the existence of small deviations ($\sim$ 0.01 mag.) in the definition of the ridge-line (using the *mean* or the *mode* of the observed colour distribution), the existence of "some" skewness in the MS star colour distribution seems reliable enough to deserve further observational checks.

Finally, Fig. 13d,e suggests that the MS IW as deduced from our data could be $0.02 \leq \sigma \leq 0.06$ mag. However, if one takes into account the existence of the quoted skewness and forces the fit to reproduce just the "blue" side of the distribution, one would get IW $\leq$ 0.02 mag as direct upper limit to the IW. On the other hand, the existence of such a skewness, if confirmed, is very interesting as it could be an indication that some optical or physical binaries exist in this cluster. Based on the present data the fraction of such objects is not high (probably less than $\sim$ 10–20%).

3.2. The RGB, and metal abundance indicators

The RGB ridge line allows the determination of various parameters related with the cluster mean metal abundance, [Fe/H], such as $\Delta V_{1.4}$ (Sandage & Wallerstein 1960) and $(B-V)_{o,g}$ (Sandage

Table 9. Metallicity and reddening values for NGC 5272

[Fe/H]	$E(B-V)$	References
—	0.00	Burstein & Mc Donald 1975
—	0.03	Kron & Guetter 1976
−1.47	—	Frogel et al. 1983
−1.32	0.01	Bica & Pastoriza 1983
−1.49	—	Geisler 1984
−1.57	—	Smith 1984
−1.43	—	Pilachowski 1984
−1.66	—	Zinn & West 1984
−1.45	—	Brodie & Hanes 1986
—	0.03	Reed et al. 1988
−1.47	—	Kraft et al. 1992

& Smith 1966). From our data we obtain $\Delta V_{1.4}$ = 2.72± 0.03 and $(B-V)_{o,g}$ = 0.77 ± 0.03 (adopting $\langle V_{HB}\rangle$ =15.63 and $E(B-V)$ = 0.01, see below). Using the calibrations of these parameters in terms of [Fe/H] proposed by Zinn & West (1984), one obtains: [Fe/H] = −1.60 ± 0.03 from $\Delta V_{1.4}$ and −1.69 ± 0.12 from $(B-V)_{o,g}$ (formal errors). These values can be compared with the latest determinations presented in Table 9, where a summary of data on M 3 are collected, and are in good agreement with [Fe/H] = −1.66 ± 0.10 (Zinn & West 1984), the value which will be adopted hereafter.

The upper limit to the IW of the RGB can be used to set an upper limit to the spread in chemical composition (and in particular on the abundance spread of low ionization potential elements, Renzini 1977). The best RGB parameter to estimate this upper limit is $(B-V)_{o,g}$. Since $\partial(B-V)_{o,g}/\partial$[Fe/H] = 0.23 mag/dex (Zinn & West 1984), an upper limit for the spread can be derived under the assumption that $\delta(B-V)_{o,g} \leq \sigma_{B-V}$, being σ_{B-V} the dispersion in colour of the RGB at the HB level. In the previous Section, we have shown that the IW of the RGB is σ_{B-V}(RGB) ≤ 0.02 mag, hence we get σ[Fe/H] ≤ 0.09 dex.

3.3. HB population and morphology

The faint end of the HB has been clearly detected at V = 17.5 and, we confirm that the total range in colour (and then in temperature) covered by the HB of M 3 is very large (see also Sandage & Katem 1982). Since the effective temperature of HB stars depends on their total and core masses (see Fig. 6 of BCF85), this evidence is a clear indication for the existence of a large spread in mass among HB stars. Rood & Crocker (1985a,b), Crocker et al. (1988), and Rood & Crocker (1989) have already widely discussed some properties of the HB stars in this cluster using our data implemented with some spectra they obtained for a small set of HB objects. Their main conclusions are that: *(i)* the stars populating the blue extension of the HB have significantly lower gravity than predicted by the standard evolutionary theory, and *(ii)* there is a significant low mass tail in the mass distribution of M 3 HB stars, as in M 15, but in this case the mass distribution is continuous. We refer to their discussion for a review of their suggested explanations for these results. Further studies, especially on the bluest objects, are being carried on by our group using IUE UV observations (Buzzoni et al. 1992, 1994b). We present in this section our present proposed interpretation of the overall HB morphology of this cluster.

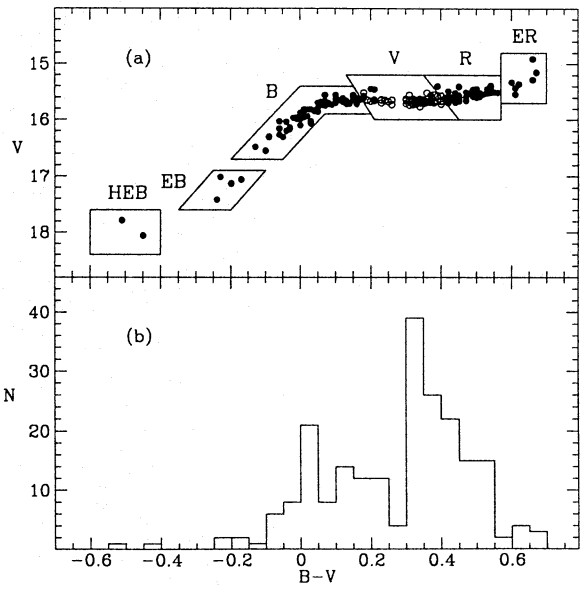

Fig. 14. a Zoomed colour-magnitude diagram of the HB including the RR Lyrae variables (Sect. 3.3.1). **b** Histogram in colour of the HB stars plotted in **a**

In order to analyse the morphology and other properties of the HB, we have identified all the variables present in the area AI+AII+AIII, where our sample CBT is complete. The average magnitudes, colours and temperatures have been taken from Table 5 of S90, whenever available, and these stars have also been used to define a period-colour relation (i.e. $B-V$ = log P_f+0.60 or $B-V$ = 0.563 log P+0.49) which has then been employed to derive the colours for the other stars not included in S90 Table 5. For the c-type variables the fundamental period has been calculated as log P_f = log P+0.125. The temperatures have been obtained from the $(B-V)$–T_e correspondence in S90.

Table 10 lists the values adopted for each variable star included in our samples (CBT, CBA). The variables marked "$(P-L)$" in the last column do not appear in S90 Table 5, and their $\langle V\rangle$ has been estimated using the pulsation equation by van Albada and Baker (1971) which relates period, mass, luminosity and temperature, on the assumption that all RR Lyrae stars in a cluster have the same mass. This relation, calibrated on S90 Table 5 data, is: m_{bol} = 54.428 − 2.975 log P − 10.358 log T_e, and allows to estimate m_V once the temperature T_e is obtained from the previous procedure and the bolometric correction is estimated from S90 Table 5 data. This relation, however, is valid only for fundamental pulsators, and for the c-type variables the average value $\langle V_c\rangle$ = 15.65 from S90 Table 5 has been adopted. Figure 14a,b presents the CMD of the HB stars in our CBT sample (including the variables) and the histogram in $B-V$ colour. Six main groups of stars can be identified:

Table 10. List of variables in the bright sample (CBT). The photometric data are from Sandage 1990 (S90) or other source as specified in the last column, when available, otherwise estimated as follows: (a) colours from a colour-period relation calibrated on the RRab and RRc data in S90 Table 5, i.e. $B-V = 0.998 \log P + 0.601$ (temperatures are then from the colour-T_e relation in S90); (b) V_{ab} magnitudes from a P–L–T relation obtained from the Van Albada and Baker (1971) pulsation equation, on the assumption that all the RR Lyrae stars in a cluster have the same mass. This relation, calibrated on the data in S90 Table 5, is: $m_{bol} = 54.428 - 2.975 \log P - 10.358 \log T_e$, and is used to derive the mean V (the BC is also estimated from S90 Table 5) once the temperature has been estimated as in (a). NB: this is better than using a PLA relation since A_b amplitudes are available only for a sub-set of stars, and A_v cannot be used in its place, being systematically smaller. The passage through the period-colour and PLT relations, however, introduces errors and the values of V, $B-V$ and T_e are less accurate for the stars labelled "(P-L)" in the last column. (c) V(RRc) = 15.65, i.e. the average value of the c-type variables in S90 Table 5 has been adopted

Variable	vZ	P	X	Y	$\langle V \rangle$	$(B-V)_{st}$	$\log T_e$	Branch	Source
1	–	.5206	−5	−129	15.67	0.32	3.829	HB	S90
5	1357	.5061	261	−23	15.64	0.31	3.832	HB[a]	NC89, (P-L)
6	361	.5143	−124	60	15.77	0.34	3.822	HB	S90
9	226	.5416	−291	−208	15.69	0.33	3.825	HB[a]	S90
10	–	.5695	154	138	15.69	0.36	3.814	HB	(P-L)
11	321	.5079	−153	−210	15.66	0.32	3.829	HB[a]	(P-L)
12	–	.3179	−4	−145	15.67	0.20	3.869	HB	S90
13	–	.4830	−26	−138	15.65	0.30	3.836	HB	(P-L)
14	–	.6359	−49	−161	15.67	0.39	3.803	HB	(P-L)
15	–	.5301	−91	−274	15.65	0.33	3.825	HB[a]	(P-L)
16	–	.5115	−301	−93	15.72	0.33	3.825	HB[a]	S90
17	–	.5761	141	−441	15.68	0.36	3.814	HB	(P-L)
18	1202	.5164	97	−296	15.71	0.35	3.818	HB[a]	S90
19	1388	.6320	350	−246	15.69	0.42	3.791	HB	S90
20	1380	.4913	333	−272	15.63	0.30	3.836	HB	NC89, (P-L)
21	1386	.5157	347	18	15.70	0.34	3.822	HB[a]	S90
22	1320	.4814	190	−11	15.66	0.30	3.836	HB	(P-L)
23	–	.5954	−113	279	15.67	0.37	3.810	HB[a]	(P-L)
24	328	.6633	−148	10	15.58	0.40	3.799	HB	S90
25	362	.4801	−124	−32	15.74	0.31	3.832	HB	S90
26	–	.5977	−178	−43	15.63	0.34	3.822	HB	S90
27	–	.5791	−110	−103	15.70	0.38	3.806	HB	S90
33	–	.5252	70	−89	15.66	0.33	3.825	HB	(P-L)
34	1265	.5591	135	170	15.68	0.35	3.818	HB[a]	S90
35	384	.5306	−108	−279	15.65	0.33	3.825	HB[a]	(P-L)
36	1308	.5456	172	−36	15.67	0.31	3.832	HB	S90
37	253	.3266	−236	165	15.66	0.24	3.856	HB[a]	S90
38	279	.5580	−203	128	15.67	0.35	3.818	HB[a]	(P-L)
39	249	.5871	−244	121	15.69	0.37	3.810	HB[a]	(P-L)
40	234	.5515	−271	112	15.70	0.34	3.822	HB[a]	S90
44	–	.5063	170	99	15.67	0.32	3.829	HB	NC89, (P-L)
45	–	.5369	−242	−130	15.67	0.34	3.822	HB[a]	(P-L)
46	–	.6134	−128	−51	15.72	0.40	3.799	HB	S90
47	–	.5410	−118	−73	15.66	0.34	3.822	HB	(P-L)
48	–	.6278	127	−103	15.57	0.39	3.803	HB	S90
49	–	.5482	140	−100	15.65	0.34	3.822	HB	(P-L)
50	–	.5136	9	−235	15.65	0.32	3.829	HB[a]	NC89, (P-L)
51	965	.5840	30	−227	15.69	0.35	3.818	HB[a]	S90
52	–	.5162	−77	152	15.64	0.32	3.829	HB	(P-L)
53	–	.5049	−7	123	15.64	0.31	3.832	HB	(P-L)
54	–	.5063	−33	106	15.67	0.32	3.829	HB	(P-L)
55	–	.5298	−203	325	15.68	0.34	3.822	HB	S90
56	–	.3296	−140	359	15.64	0.23	3.860	HB	S90
57	–	.5122	155	−1	15.65	0.32	3.829	HB	(P-L)
59	378	.5888	−110	−229	15.69	0.37	3.810	HB[a]	(P-L)
60	–	.7077	−298	−316	15.55	0.38	3.806	HB	S90
61	1321	.5209	190	364	15.63	0.32	3.829	HB	(P-L)
63	–	.5704	38	342	15.69	0.36	3.814	HB[a]	(P-L)

Table 10. (continued)

Variable	vZ	P	X	Y	$\langle V \rangle$	$(B-V)_{st}$	$\log T_e$	Branch	Source
64	–	.6055	115	330	15.67	0.36	3.814	HB[a]	S90
65	–	.6683	126	328	15.52	0.36	3.814	HB[a]	S90
66	–	.6202	−101	121	15.67	0.38	3.806	HB	(P-L)
67	–	.5684	−131	123	15.64	0.35	3.818	HB	(P-L)
68	–	.4785	22	175	15.65	0.26	3.849	HB[c]	NC89, $V = V_c$
69	–	.5666	81	141	15.66	0.35	3.818	HB	(P-L)
70	1003	.4861	38	152	15.65	0.30	3.836	HB	NC89, $V = V_c$
71	–	.5491	160	−3	15.73	0.32	3.829	HB	S90
74	–	.4921	88	151	15.71	0.30	3.836	HB	S90
75	–	.3141	49	159	15.70	0.23	3.860	HB	S90
79	–	.4833	44	350	15.65	0.30	3.836	HB[a]	(P-L)
84	–	.5957	64	165	15.67	0.40	3.799	HB	S90
85	1373	.3558	306	226	15.52	0.18	3.876	HB	S90
87	–	.3575	110	60	15.65	0.26	3.849	HB[c]	$V = V_c$
89	–	.5485	28	−111	15.65	0.34	3.822	HB	(P-L)
90	–	.5170	97	−189	15.68	0.36	3.814	HB[a]	S90
92	–	.5036	−30	−409	15.64	0.31	3.832	HB	(P-L)
95	318	102.1	−155	15	12.36	1.78		AGB	Welty
96	–	.4994	−164	−234	15.56	0.31	3.832	HB[a]	S90
97	353	.3349	−130	−197	15.65	0.24	3.856	HB[a]	$V = V_c$
99	1330	?	201	−55				HB[b]	
100	–	.6188	70	97	15.68	0.38	3.806	HB	(P-L)
102	–	?	58	115				HB[b]	
104	–	.5699	−26	145	15.68	0.36	3.814	HB	(P-L)
105	679	.2877	−21	191	15.60	0.18	3.876	HB	S90
106	–	.5472	−48	168	15.65	0.34	3.822	HB	(P-L)
107	–	.3090	−75	336	15.66	0.21	3.866	HB[a]	S90
108	–	.5196	−218	311	15.71	0.32	3.829	HB	S90
118	1277	.4994	144	−293	15.65	0.31	3.832	HB[a]	(P-L)
119	–	.5177	253	106	15.64	0.30	3.836	HB[a]	S90
120	–	.6401	−295	232	15.66	0.40	3.799	HB	S90
124	479	.7524	−66	−202	15.57	0.40	3.799	HB[a]	S90
125	–	.3498	186	−133	15.68	0.25	3.853	HB[a]	S90
126	–	.3484	−16	−147	15.73	0.26	3.849	HB	S90
128	–	.2920	114	131	15.65	0.19	3.873	HB	NC89, $V = V_c$
138	238	80.98	−263	41	12.71	1.56		AGB[a]	Welty
140	–	.3331	−16	109	15.65	0.23	3.860	HB	S90
202	190	.999:	−378	97	15.55	0.46	3.774	HB	Cudworth
203	632	.2872	−28	−312	15.57	0.15	3.886	HB[a]	Cudworth
209	472	.3529	−68	−99				HB	C91
225	837	89.59	8	225	12.68	1.50		AGB[a]	Welty
—	1313	?	179	−14	14.04	0.99		AGB	Cudworth
—	430	?	−84	−398	15.14	0.76		AGB	Cudworth

[a] Variables included in the CBA sample;
[b] presumably RR Lyrae variable;
[c] double-mode pulsator, see NC89 for secondary period; S90: Sandage 1990, ApJ 350, 603; Welty: Welty 1985, AJ90, 2555; Cudworth: Cudworth 1979, AJ 84, 1312; (P-L): from the P-L-T relation, see text; $V = V_c$: the average $V_c = 15.65$ has been adopted; C91: Carretta 1991, Thesis, Univ. of Bologna; NC89: updated period by Nemec and Clement 1989, AJ 98, 860.

(1) Group R: 51 objects, including all the HB stars redder than the red edge of the instability strip (at $B-V = 0.42 \pm 0.02$) and bluer than the small gap (at $B-V = 0.58$) which separates the HB from the set of 7 stars which appear to be climbing towards the AGB (defined below as ER);

(2) Group ER: 7 objects in total, including the HB stars redder than the quoted small gap at $B-V = 0.58$ and fainter than $V = 14.8$;

(3) Group V: 90 objects, including all the RR Lyrae variable stars (see Table 10);

(4) Group B: 70 objects, including all the HB stars bluer than the blue edge of the instability strip (at $B-V = 0.18 \pm 0.02$) and redder than the gap (at $B-V = -0.13$) which separates the bulk of the blue HB population from the blue tail;

(5) Group EB: 4 objects (in sample CBT) with $B-V < -0.15$ and $V > 17$ (see Fig. 14);

(6) Group HEB: including the two stars with $B-V < -0.35$ (where actually the $B-V$ colour index approaches saturation) and $V \sim 18$, not shown in Fig. 14 (see Fig. 10 and 11).

The reason for such a subdivision is to understand the origin and evolutionary status of the various groups, and distinguish between the two main alternatives: *(a)* all the groups are formed by true HB members evolving through a normal HB evolutionary stage; then one must search for the parameter(s) which produce the observed modulation in their distribution; or *(b)* at least some group is made of peculiar objects which do not experience a normal HB evolution but populate the HB due to the combination of other factors; in other words, the modulations or discontinuities in the $B-V$ distribution in Fig. 14b are due to the presence of "multiple" stellar populations on the HB (Crocker et al. 1988; Rood & Crocker 1989).

We are inclined to favour the second possibility, in particular we suggest that group HEB stars are actually Post-HB members, while the ER objects might represent the progeny of some of the blue stragglers found above the TO region (see Fusi Pecci et al. 1992). To explain the reason of this choice we analyse briefly the various groups, starting from those for which there is little doubt that they represent *bona fide* HB stars.

3.3.1. Groups B, V, and R

These three groups represent 95% of the total population of candidate HB members with population ratios $B : V : R = 70 : 90 : 51$ (Fig. 14a). They cover a colour range $-0.13 < (B-V) < 0.58$ with a mean 1σ vertical dispersion of about 0.05 mag around the ridge line.

The mean V-magnitude for the 96 RR Lyrae variables here considered is $\langle V_{RR} \rangle = 15.66 \pm 0.05$ (S90), while using the non-variable stars we have obtained $V_{be} = 15.66 \pm 0.02$ and $V_{re} = 15.61 \pm 0.02$ for the blue and red edge of the instability strip, respectively. Note that there is a tiny off-set in the zero-point between the adopted magnitudes for the variable and constant stars which will be analysed and discussed in the following papers of this series.

Taking into account that evolution leads HB stars to brighten slightly with respect to the ZAHB level and that most of the HB lifetime is expected to be spent close to the ZAHB, we have chosen as representative of the "real" ZAHB level the average of the three values determined above – V_{RR}, V_{be}, V_{re} – arbitrarily increased by 0.01 mag to allow for some evolution off the ZAHB. Therefore we adopted $V_{ZAHB} = 15.65 \pm 0.05$. Note however that following Sandage (1993c) precept $\Delta V = V_{ZAHB} - \langle V \rangle = 0.05[Fe/H] + 0.16$ this value would be $V_{ZAHB} = 15.72 \pm 0.05$.

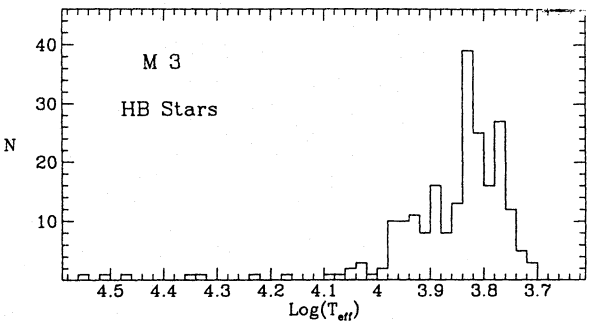

Fig. 15. Distribution of HB stars in effective temperature, computed using the model atmospheres from Kurucz (1979, Table VB), $E(B-V) = 0.01$, $\log g = 3.0$ and [Fe/H] $= -1.66$

The histogram of Fig. 14b can be translated from colours to effective temperatures using the model atmospheres computed by Kurucz (1979) (his Table 5b) and assuming $E(B-V) = 0.01$ and [Fe/H] $= -1.66$. The results are shown in Fig. 15. As widely discussed by BCF85 and Fusi Pecci et al. (1993a,b), the observed asymmetric distribution of the HB towards a blue tail could be due to various reasons related to the different mass lost during its previous evolution by each individual HB star. For instance, if a Gaussian distribution of the rotating core angular velocity is envisaged, a small dispersion around the mean value could be enough to produce a skewed HB star distribution with blue HB tails as a result of the chain: higher rotation → higher core mass → higher mass loss → smaller ZAHB mass → bluer ZAHB colours (Renzini 1977; Fusi Pecci & Renzini 1978). Alternatively, the existence of the blue tail could be caused by an enhanced mass removal from the HB progenitors, possibly due to increased interactions between the stars in the denser cluster environments (Fusi Pecci et al. 1993a,b).

3.3.2. Group EB

The presence of these four stars clearly separated from the main body of the HB members puts M 3 into the growing number of clusters presenting this "unexpected" feature in the HB population (see for instance Fusi Pecci 1987, Table II). Due to the small number of EB stars, we cannot exclude that this clump is simply a stochastic fluctuation in the overall distribution. Other explanations are however possible, suggested by a growing body of observational evidences, such as the colour and population radial gradients in various post-core collapsed clusters (see for references Piotto et al. 1988; Bailyn et al. 1988, 1989; Djorgovski et al. 1988, 1991a,b; Stetson 1991; Djorgovski & Piotto 1992; Cederbloom et al. 1992). These data seem to indicate that there is a connection between the present HB morphology and

the global dynamical evolution of the stars within the cluster environment (see Fusi Pecci et al. 1993a,b for a discussion).

Very schematically, there are two main paths (which may also coexist) along which the interaction between dynamics and stellar evolution can take place:

(a) A subset of the present blue HB stars may have lost more mass than normal HB stars due to some still unknown mechanism somehow related to the central stellar density of the cluster (Renzini 1983; BCF85; Fusi Pecci 1987; Fusi Pecci et al. 1993a,b). Note that in M 3 the difference in mass between the bluest HB stars in group B and the EB stars is less than 0.04 $M_{\odot}$ (Rood & Crocker 1989, Fig. 14).

This scenario is supported by the comparison between the HB morphologies of NGC 5466 and M 15 (BCF85), which are very similar in many respects but have low and high density, respectively: M 15 displays a large population of EB stars (sometimes referred to as blue subdwarfs, sdBs, Bailyn 1992) which are totally absent in NGC 5466. Moreover the population ratios between the main branches in the CMDs of these two cluster would be difficult to understand if the stars populating the blue HB tail in M 15 were "non-genuine" HB objects (BCF85).

(b) These EB stars (or sdBs) are the result of the merging of binary systems made of helium white dwarfs which could evolve into contact through gravitational radiation (Grindlay et al. 1981; Iben & Tutukov 1986; Bailyn et al. 1988; Bailyn & Iben 1989; Iben 1990). Alternatively some sdBs might result also from mass transfer from a giant star in a pair prior to core flash (Mengel et al. 1976; Bailyn 1992).

The strongest support for the binary nature of EB stars is given by the increasing observational evidence that the EB stars display frequently different radial distributions compared to all the other "normal" stars and that colour gradients exist in many clusters (see Stetson 1991; Djorgovski & Piotto 1992, and Bailyn 1992 for references). However the data, still rather meager on these stars, do not converge unanimously to the same conclusion. For instance, in M 15 (BCF85, Stetson 1991), NGC 6752 (Buonanno et al. 1986), and M 71 (Drukier et al. 1989) the EB stars in the outer regions of the clusters are at least as frequent as (or even more than) in the inner areas, a part the very central regions not properly surveyed yet.

3.3.3. Group ER

These stars are traditionally interpreted either as normal HB objects which lost less mass than the mean cluster population during the RGB phase for some unknown reason (just the opposite of group EB members), or as evolved HB stars. Both interpretations are consistent with the HB synthetic models. (e.g. by Lee et al. 1990). However, the latter hypothesis seems weaker, as ZAHB stars with the M 3 metallicity evolve at significantly brighter luminosities than these seven stars (Sweigart & Gross 1976; Gingold 1974,1976). If interpreted as ZAHB stars, their total mass should be larger than 0.85 $M_{\odot}$. If these stars were included into the sample of normal HB stars, the population ratios would become: $(B + EB) : V : (R + ER) = 74 : 90 : 58$.

The reason why we have singled them out as a special group stems from the possibility that these objects may represent the "daughters" of the BSS (see Fusi Pecci et al. 1992)

3.3.4. Group HEB

This group includes only two stars in our sample, i.e. *524=I-III-87* and *7561=I-V-37*, which are the faintest and the bluest HB candidates, but we believe that they are actually Post-HB stars located on the extension of the HB locus in the CMD because of the large bolometric correction due to their very high effective temperature. To clarify definitely the intrinsic nature of these objects, we have observed them with the IUE-satellite, and the values of temperature and luminosity we have derived suggest that these objects are not normal HB members, but are likely to be post-HB stars of the type ABG-manqué or the progeny of late collisional mergers (see Buzzoni et al. 1992 for more details).

The number of UV-bright stars in M 3 includes 4 other stars. One of them is the brightest star *156* in our catalogue, which is the well-known Post-AGB star *Von Zeipel 1128 = I-II-57*, two (*352 = I-I-58* and *843 = I-IV-54*) belong to the group EB, and one (*621 = I-III-57*) is the bluest star in our B sample. The importance of the study of these stars has been frequently stressed while examining problems such as the UV-excess in elliptical galaxies (Burstein et al. 1988; Greggio & Renzini 1990; Davidsen & Ferguson 1992; Bertola et al. 1993, and references therein). In a forthcoming paper (Buzzoni et al. 1994b) we will present the results of the IUE observations of these stars, as well as discuss their influence on the contribution to the integrated light of the sampled population.

3.4. Helium abundance

The HB and AGB phases of evolution are higly influenced by the still uncertain treatment of mixing phenomena and mass loss. Since the evolution on the RGB occurs before the onset of their strong effects, and the population ratios of these three branches can provide an observational determination of the HB and AGB lifetimes, a comparison with the theoretical lifetimes provides an estimate of these parameters via proper calibrations (see for a discussion: BFBC, Castellani et al. 1985; Bressan et al. 1986; Renzini & Fusi Pecci 1988).

Four ratios can be defined:

(1) $R = N_{\rm HB}/N_{RGB}$, where $N_{\rm HB}$ and N_{RGB} are respectively the number of stars on the HB and on the RGB above the luminosity of the HB.

(2) $R' = N_{\rm HB}/(N_{RGB}+N_{AGB})$, where N_{AGB} is the number of stars in the AGB phase.

(3) $R1 = N_{AGB}/N_{RGB}$.

(4) $R2 = N_{AGB}/N_{\rm HB}$.

The main difficulty in the estimate of these ratios is the separation of the various branches, in particular the definition of the base of the AGB and RGB.

Following the procedure described in BFBC, we fixed the separation between HB and AGB at about 0.8 magnitude above the HB. This choice makes the present values homogeneous

Table 11. Star counts in RGB, HB and AGB

N_{RGB} = 165	R = 223/165 = 1.35±0.20
N_{HB} = 223	R' = 223/204 = 1.09±0.15
N_{AGB} = 39	$R1$ = 39/165 = 0.24±0.06
	$R2$ = 39/223 = 0.17±0.04

with the previous ones obtained by BFBC from the Sandage and Katem (1982) diagram. The level of the RGB down to which the counts should be extended was fixed taking into account a differential bolometric correction between HB and RGB stars ΔBC=0.22 mag. A standard mean value of 0.15 mag (as used in BFBC) would have decreased the RGB counts by a factor of 7.8% (from 165 to 152).

Table 11 presents the number of stars we derived from our complete sample CBT and the ratios R, R', $R1$ and $R2$. The values of $R1$ and $R2$ confirm the result obtained by BFBC and, in particular, confirm the existence of a fully developed semiconvection zone as predicted by the so-called "standard and canonical" models (for instance Sweigart & Gross 1976, Sweigart et al. 1987). These ratios are also compatible with the models with overshooting computed by Bressan et al. (1986). while they would tend to exclude the existence of the so-called *breathing pulses* suggested by Castellani et al. (1985). However, their actual physical nature has been recently put in doubt by Castellani et al. (1989), and excluded by Dorman & Rood (1992).

Once the HB lifetimes of the standard and canonical models have been adopted, one can use the so-called R-method (Iben 1968) to get a direct estimate of the primordial helium abundance, Y. Note that what matters in order to estimate the helium abundances from the $(R-Y)$-calibration is the knowledge of the RGB and HB lifetimes, and not necessarily the knowledge of the mixing mechanism at work in HB stars. Since only the existence of pronounced and long breathing pulses may alter the lifetimes adopted in the $(R-Y)$-calibration, while *overshooting* does not affect the calibration significantly, we believe that the $(R-Y)$-calibration proposed in Eq. (11) of BFBC still represents the best formula to use.

We obtain therefore $Y = 0.23 \pm 0.02$ (where the error refers only to the count statistics). The use of R' (see Eq. (12) of BFBC) would lead to $Y = 0.23 \pm 0.03$, in perfect agreement. This result is based on the assumption that the non-genuine HB stellar population, if any, is very small indeed and this effect on the stellar ratios is well within the observational error.

3.5. The main sequence and the cluster age

As first noticed by Eggen & Sandage (1969), and later further commented by Sandage & Katem (1977), a gap has been found at $M_V \sim +5$ in some old open clusters (see Bonifazi et al. 1991 and references therein), due to the hydrogen exhaustion at the core. No gap is expected in globular clusters because the $p-p$ chain presumably dominates over the CNO-cycle, and a convective core is absent. One of the original purposes of this work was to investigate the upper main sequence to verify this theoretical expectation.

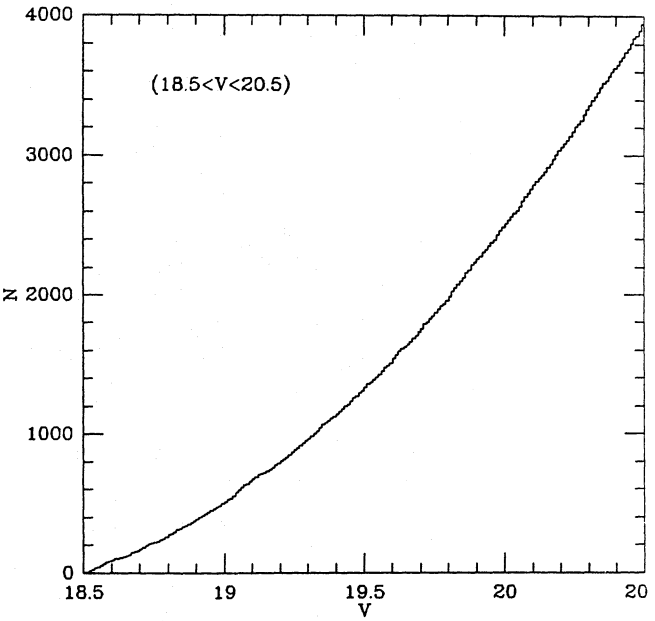

Fig. 16. Cumulative luminosity distribution in the Turn-Off region to check for the possible existence of gaps or clumps. The smooth shape of the distribution seems to exclude them at a quite high confidence level (Sect. 3.5)

The present MS is so highly populated and the internal photometric accuracy in the turnoff region is so good that we decided to explore this occurrence since a gap, if present, could hardly escape detection. As it can be seen from Fig. 16, where we display the cumulative star counts in the turnoff region, no significant evidence of "discontinuities" (and then of gaps in the differential luminosity function) are present, confirming the validity of the models.

Three other aspects are then important:

(i) the age of the cluster as deduced from the TO-luminosity and from the whole MS;

(ii) the intrinsic width of the MS, in order to study both chemical homogeneity and possible effects due to rotation or binaries (if any);

(iii) the luminosity function, to have hints on the slope of the present and initial mass function and to make comparisons with the models.

We have already presented in Sect. 3.1.2 some indications on item (ii) that can be derived from the present data, but we postpone the complete analysis of both points (ii) and (iii) to the forthcoming papers which make use of the CCD data.

Concerning point (i), as we have already analysed the problem of age estimates separately (BCF89, Buonanno et al. 1990; Sandage & Cacciari 1990) by considering a photometrically homogeneous sample of 19 Galactic globular clusters, we shall not repeat that analysis here but only report the results for M 3.

Table 12. Previous age estimates for M3 based on the present original data

Reference	Method	Calibration	$E(B-V)$	[Fe/H]	[O/Fe]	V_{HB}	V_{TO}	ΔV_{HB}^{TO}	$(m-M)$	t_9
BCF89	ΔV	VdBB85 isoc. + $+M_V$(HB) = 0.37[Fe/H] + 1.29	0.01	−1.66	0.00	15.65	19.17	3.52	14.94[a]	18.7
SC90	MS-fit	VdBB85 isoc.	0.01	−1.66	0.00	15.62	19.07	3.45	14.81[a]	18.6
	MS-fit	VdBP89 isoc.			0.63					14.0
	ΔV	VdBB85 + $+M_V$(RR) = +0.8	0.01	−1.66	0.00	15.62	19.07	3.45	14.82[a]	18.4
					0.00	15.62	19.17	3.54		20.1
					0.63	15.62	19.07	3.45		14.8
	ΔV	VdBB85 + $+M_V$(RR) = 0.19[Fe/H] + 1.13	0.01	−1.66	0.00	15.62	19.07	3.45	14.81[a]	18.6
					0.00	15.62	19.17	3.54		20.2
					0.63	15.62	19.07	3.45		15.0
	ΔV	VdBB85 + $+M_V$(RR) = 0.39[Fe/H] + 1.27	0.01	−1.66	0.00	15.62	19.07	3.45	15.00[a]	15.5
					0.00	15.62	19.17	3.54		16.9
					0.63	15.62	19.07	3.45		12.5
CS89	Fit	CS89 isoc.	0.03	−1.6	0.00				15.01[b]	14
			0.00	−1.6	0.00				14.95[b]	16
			0.00	−1.6	0.00				14.90[b]	18
VdBBS90	$\Delta(B-V)$	Differential	Age ≃ NGC 6752, NGC 7492, M12, and 1-2 Gyr < M13							
SC91	Fit	SC91 isoc.	0.01	−1.62	0.00				14.91[b]	19
CSJ92	ΔV	RYI87 isoc., BC(TO)=-0.21 + $+\langle M_V(\mathrm{RR})\rangle$ = 0.15[Fe/H] + 1.01	0.01	−1.66	0.30	15.65	19.17	3.52		17.0
					0.91					14.2
W92	ΔV	VdBB85 isoc. + $+\langle M_V(\mathrm{RR})\rangle$ = 0.15[Fe/H] + 0.73	0.01	−1.66	0.41	15.65	19.17	3.52		13.7
CSD92	ΔV	CSD92 isoc. [diffusion] + $+\langle M_V(\mathrm{RR})\rangle$ = 0.17[Fe/H] + 0.82	0.01	−1.66	0.40 *	15.65	19.17	3.52		14.2 [d]
										13.8 [e]
SCS93	ΔV	SCS92 isoc. [α/Fe] + $+M_V$(HB) = 1.1595 + 0.5047[M/H] + +0.086[M/H]^2	0.01	−1.66	0.00	15.65	19.17	3.52		16.1
					0.60[c]					15.6
	$\Delta(B-V)$	idem	0.01	−1.29	0.60[c]	15.65	19.17	3.52		18
S93	ΔV	BVdB92 isoc. [O/Fe] + $+M_V$(HB) = 0.94 + 0.30[Fe/H]	0.01	−1.66	0.63	15.62	19.07	3.45		14.0

References: BCF89 (Buonanno, Corsi & Fusi Pecci 1989); VdBB85 (VandeBerg & Bell 1985); SC90 (Sandage & Cacciari 1990); VdBP89 (VandenBerg & Poll 1989); VdBBS90 (VandenBerg, Bolte & Stetson 1990); CS89 (Chieffi & Straniero 1989); SC91 (Straniero & Chieffi 1991); CSJ92 (Carney, Storm & Jones 1992); RYI87 (*Revised Yale Isochrones*, Green, Demarque & King 1987); W92 (Walker 1992); CSD92 (Chaboyer, Sarajedini & Demarque 1992); SCS93 (Salaris, Chieffi & Straniero 1993); S93 (Sandage 1993a,b,c); BVdB92 (Bergbush & VandenBerg 1992)

Notes: [a] $(m-M)_0$; [b] $(m-M)_V$; [c] [α/Fe]; [d] no helium diffusion; [e] with helium diffusion

Moreover, since the publication of our SGB and MS mean loci, our data have been used by various Authors to estimate the cluster age using different assumptions and methods. Therefore, it may be interesting to summarise and compare here all the previous results obtained on the basis of the present data. In particular, we note that the quite stricking discrepancies existing amongst the various age determinations *based on the same original data* (see Table 12) simply reflect the uncertainties in the various assumptions and calibrations necessary to link the apparent magnitude of the TO to the absolute age.

Buonanno et al. (1989). The basic age-observable parameter we have deduced from our CMD of M 3 is $\Delta V_{TO}^{HB} = 3.52 \pm 0.09$, from $V_{HB} = 15.65 \pm 0.05$ and $V_{TO} = 19.17 \pm 0.07$. This value is totally compatible with the average $\Delta V_{TO}^{HB} = 3.55 \pm 0.09$ obtained for the 19 clusters included in the studied sample.

A constant value of ΔV_{TO}^{HB} may lead to coevality for all the clusters or to large age differences depending on the slope adopted for the M_V^{HB} vs. [Fe/H]-relation and on the scaling of the heavy element abundances relative to iron. Furthermore, the absolute age depends strongly on the zero-point of the luminosity-metallicity relation which was adopted to be 1.29.

We obtained the distance modulus $(m-M)_0 = 14.94 \pm 0.25$ and age $t = 18.7 \pm 3.5$ Gyr, where the errors are a conservative global estimate of the errors due both to observations and calibrations. An O-enhancement [O/Fe] = +0.3 would decrease the age by about 1 Gyr.

The assumptions at the base of this results are: *i)* the slope is $\Delta M_V^{HB}/\Delta[Fe/H] \sim 0.35$, and *ii)* the zero-point is 1.29, based on a MS-fitting to the small set of available metal-poor subdwarfs with known trigonometric parallaxes (Lutz et al. 1987).

Sandage & Cacciari (1990). Using the MS locus published in Table 2 of BCF89, these authors have derived the cluster age using three different assumptions for the M_V^{HB} vs. [Fe/H]-relation, the observed ΔV_{TO}^{HB} or a mean $\langle \Delta V_{TO}^{HB} \rangle = 3.54$, and taking into consideration or not [O/Fe] enhancements (see their Tables 3,4,5). The derived ages range from 12.5 up to 20.2 Gyr, showing that our conservative estimate of the error on the absolute age (i.e. 3–4 Gyr) could even be optimistic.

VandenBerg et al. (1990). The new method they proposed, now referred to as the $\Delta(B-V)$-method, aims at the determination of *relative* ages and is based on the determination of the proper displacement in magnitude and colour necessary to superimpose the MS-TO regions of two clusters having the same metal content. Then, one can use theoretical calibrations computed as a function of age and chemical composition (including non-solar scaling of the heavy elements) to estimate the difference in age of the two compared clusters. Such a procedure has been applied by these Authors to compare the mean locus of M 3 with NGC 6752, M 12, NGC 7492, and M 13 assumed to belong to the same metallicity group with [m/H] ~ -1.6.

They conclude that: (i) "there is clearly no compelling evidence that any one of the clusters is different in age from any other"; and (ii) "the close coincidence of the M 3 CMD with that of NGC 6752 suggests that age is unlikely to be the only (or main) cause of the so-called *second parameter* effect – the wide diversity in HB morphologies among GCs of the same metallicity". Considering that the CMD of NGC 6752 displays a very long blue HB tail with a gap (Cannon 1981; Buonanno et al. 1986) and that NGC 7492 has a galactocentric distance of ~ 18.8 kpc (Thomas 1989) this result, if confirmed, represents quite a strong proof against the overall description and interpretation of the second parameter problem currently supported by the Yale Group mostly (if not exclusively) in term of age differences (see Lee 1992 and references therein, and Fusi Pecci et al. 1993b for further discussions).

The comparison with M 13 is less stringent (their Fig. 11), as the quality of the available M 13 data is insufficient. However this comparison would rather suggest a difference in age of about 1–2 Gyr between M 3 and M 13 (with M 13 being older) in order to explain the observed difference in HB morphologies, in agreement with the scenario proposed by the Yale Group.

Chieffi & Straniero (1989) and Straniero & Chieffi (1991). Using their new set of standard (i.e. solar-scaled abundances) isochrones Chieffi & Straniero (1989) have shown various best fitting solutions for M 3 spanning a range in age between 14 and 18 Gyr and apparent distance modulus $14.90 < (m-M)_V < 15.01$. Their conclusion is that with their adopted parameters the various fits reproduce reasonably well the observed shape of the whole CMD of the cluster (a part from the upper part of the giant branch), but that it is not possible to reduce the error in the absolute age determination below 2–3 Gyr.

Straniero & Chieffi (1991) have further refined their analysis and found an age of 19 ± 1 (see Table 12).

Carney et al. (1992). Using the RR Lyrae luminosity-metallicity relation $\langle M_V(RR) \rangle = 0.15[Fe/H] + 1.01$ and a bolometric correction -0.21 for the TO, they have determined the age of M 3 based on the Revised Yale Isochrones (Green et al. 1987) and assuming two different options for the [O/Fe] enhancement. For $[\alpha/Fe] = [O/Fe] = +0.3$, they have obtained 17.0 ± 1.5 Gyr, and for $[O/Fe] = -0.42[Fe/H] + 0.22$ the resulting age decreased to 14.2 ± 1.0 Gyr.

Walker (1992). From the study of 182 RR Lyrae variables in seven Large Magellanic Cloud clusters, Walker has obtained a new independent estimate of the zero-point in the $M_V(RR)$–[Fe/H] relation based on the distance modulus to the LMC assumed to be 18.5 ± 0.1, where the slope was adopted from Carney et al. (1992). This relation, i.e. $\langle M_V(RR) \rangle = 0.15[Fe/H] + 0.73$, yields magnitudes almost 0.3 mag brighter than Carney et al. (1992) and just above 0.2 mag brighter than BCF89 at [Fe/H] = -1.66 for M 3. Using our data and taking into account also the possible changes in [O/Fe], Walker derives then an age of 13.7 Gyr for M 3.

Chaboyer et al. (1992) In order to evaluate the importance of helium diffusion on cluster ages, claimed until recently to be able to decrease the absolute age by about 30% (Stringfellow et al. 1983), these authors have computed a wide set of new isochrones taking into account the effects of microscopic diffusion of helium with various recipes. In addition, the abundances of α-

elements were enhanced with respect to Fe by +0.4 to take into account the element to element variations observed in field and globular cluster stars. Then, to estimate the absolute ages of 20 clusters (including M 3 using our data), they applied the $\Delta V_{\rm TO}^{\rm HB}$-method adopting the relation $\langle M_V({\rm RR})\rangle = 0.17[{\rm Fe/H}] + 0.82$. From the standard models (i.e. no diffusion) they estimated an age of 14.2 ± 1.3 Gyr for M 3, which may decrease to 13.8 if diffusion is included.

Salaris et al. (1993). The major aspect pointed out by these Authors in re-computing a new set of theoretical isochrones is that, if non-solar scaled abundances for the α-elements are considered, the effects produced by the elements other than oxygen cannot be neglected as done in most of the previous computations used to estimate the ages reported above. If opacities and nuclear reaction rates are properly dealt with, the absolute ages of the clusters are only mildly affected by the enhancement of the α-elements. In particular, while for [CNO/Fe] = +0.3 the absolute age decreases by about 1 Gyr if the Bergbush & VandenBerg (1992) isochrones are used (where only the Oxygen abundance has been enhanced), the difference is negligible using Salaris et al. isochrones and the $\Delta(B-V)$-method, and is at most 0.7 Gyr (but decreasing with increasing metallicity) if the $\Delta V_{\rm TO}^{\rm HB}$-method is adopted.

Therefore using our original data and the $M_V({\rm HB}) - [{\rm Fe/H}]$ relation computed by Castellani et al. (1991) (which is parabolic instead of linear as usually adopted), these authors have obtained for M 3 absolute ages of 16.1 Gyr for [α/Fe] = 0, and 15.6 Gyr for [α/Fe] = +0.6. Though much more uncertain, they have also computed the age using the $\Delta(B-V)$-method obtaining for the α-enhanced case an age of about 18 Gyr.

Sandage (1993a,b,c). In a recent series of papers, Sandage (1993a,b,c) has presented a new calibration of the RR Lyrae absolute luminosity as a function of metallicity which is brighter by ~ 0.25 mag . This new calibration, i.e. $M_V = 0.30[{\rm Fe/H}] + 0.94$, coupled with the age-equation $Logt = 0.39 M_{\rm bol}^{TO} - 0.10[{\rm Fe/H}] + 8.441$ obtained from the O-enhanced isochrones computed by Bergbush & VandenBerg (1992), yields for M 3 a brighter HB luminosity, a smaller distance and a younger age than previously obtained. In particular, Sandage (1993c) derives for M 3 an age of 14.0 and 13.1 Gyr, based on the data listed in Sandage & Cacciari (1990) and BCF89 respectively.

M 3 age as derived from other original data. Considering only the latest studies on cluster ages reporting specific figures or tables on the age of M 3 based on original data different from those here presented (we recall that our MS ridge line has been published in Table 2 of BCF89), one gets a similar spread in the derived absolute ages depending on the assumptions and on the method adopted.

In particular, Sarajedini & King (1989) based on data by Peterson (1986) obtained an age of 12.4 ± 1.5 if the Lee et al. (1990) synthetic $M_V({\rm HB}) - [{\rm Fe/H}]$ relation is adopted, 14.6 ± 1.8 Gyr if $M_V({\rm HB}) = +0.6$ is assumed, and, finally 17.6 ± 2.2 Gyr if the Sandage (1982) relation $\langle M_V({\rm RR})\rangle = 0.35[{\rm Fe/H}] + 1.39$ is taken.

Paez et al. (1990) presented new CCD photometry for about 5000 stars down to $V \sim 23$, and derived age and distance modulus estimates by fitting the observed mean ridge lines to the theoretical isochrones computed by Chieffi & Straniero (1989). They obtained a best matching between observational and theoretical quantities for $14.85 < (m-M)_V < 14.95$ and $16 < t_9 < 19$.

Straniero & Chieffi (1991) have also applied their dating procedure to the CCD data obtained by Paez et al. (1990). Note that their fiducial MS is similar in shape to our own but systematically red shifted by about 0.02 mag and they concluded that a global solution leading to consistent values of age, distance modulus and reddening with our data set would imply quite a high metal content, [m/H] = −1.29, marginally compatible with most observational data.

Conclusions on the age of M 3. It is quite evident from the above survey of the latest age determinations made with different methods and assumptions that, even starting from the same data base, one may derive quite a large range of values. This is highly indicative of the uncertainties still affecting any dating procedure.

In conclusion, the problem of determining accurately the absolute age of M 3 is still open. Several estimates made via different procedures and calibrations converge towards a value ($t \geq 14$ Gyr and frequently $\sim 16 - 17$ Gyr) which is considered still high, at least for what concerns some cosmological implications, however some of the most recent results seem to suggest values ≤ 14 Gyr.

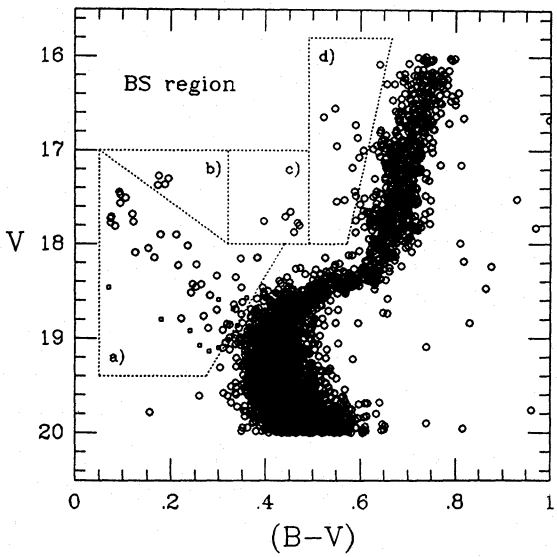

Fig. 17. Zoomed colour-magnitude diagram of the region of the blue stragglers. The dotted lines define the separation into various sub-groups discussed in the text in Sect. 4.2. Small symbols denote objects with worse photometric quality (sample FA2)

4. The blue stragglers

4.1. Overview

The BSS first identified as a specific population by Sandage (1953) in M 3, form an extension of the MS up to about 2–2.5 mag brighter than the MS-TO and are easily detectable in the CMD shown in Fig. 10, thus confirming Sandage's early results.

Until recently, only a few other loose clusters presented a comparable population of BSS. Nowadays, many BSS candidates have been detected in several clusters, including the very central regions of highly concentrated globulars like 47 Tuc (Paresce et al. 1991), NGC 6397 (Aurière et al. 1990; Lauzeral et al. 1992), and M 15 (Ferraro & Paresce 1993). Fusi Pecci et al. (1992) have presented a catalog listing 425 BSS in 21 Galactic globular clusters, which is however incomplete as new detections are continuosly reported in almost any cluster purposely surveyed (see for instance Sarajedini 1993).

The present photometric study has allowed us to identify several new BSS candidates in addition to those already found by Sandage (1953). They are shown in Figure 10 and 17 and listed in Table 13. The separation between the MS and the BSS population around the TO region is somewhat uncertain and subjective. As a consequence, the total number of BSS is a function of how the discrimination has been made. Figure 17 shows a zoomed plot of the TO region in the CMD. The dotted line delimiting area "a" indicates the adopted separation between the MS and the BSS stars, and this area includes the objects which we define to be *bona fide* BSS candidates.

There are however a few other stars located outside area "a" and to the blue of the MS and SG-RG branches, which are worth some attention, namely the stars at $V = 17.3$, $B - V = 0.2$ (4 stars, group "b"), those at $V = 17.8$, $B - V = 0.5$ (6 stars, group "c"), a sparse group of objects slightly brighter than the brightest BSS ($V \sim 16$–18) and located to the blue of the faint RGB (group "d"), and a small group fainter than the MS-TO and much bluer than the MS itself. Their photometry has been repeatedly checked and their nature requires further discussion.

It cannot be excluded that these stars are contaminating field objects, as one can estimate from the counts of field stars by Ratnatunga & Bahcall (1985, Table 2A) for $B - V < 0.8$ and $V < 19$. An alternative explanation for most of the stars located in the areas "b", "c", and "d" is that they are optical blends, which are rather frequent in very crowded fields observed in "medium" seeing conditions. This possibility, supported by the fact that most of these objects display the worst photometric quality, has been carefully evaluated also by comparison with similar objects found in the CMD's of the clusters we have subsequently studied (see for instance NGC 6171, Ferraro et al. 1992a; NGC 1904, Ferraro et al. 1992b; NGC 5897, Ferraro et al. 1992c). We have devised a procedure to estimate (via simulations) which "optical" combinations of normal stars located along the main branches could produce the resulting blended objects. We present in Fig. 21a–f a set of simulated de-blended objects which might explain the various sub-sets of stars in M 3. No reasonable solution has been found for the 4 stars membering sub-group "b", and therefore we believe that they are real "single" stars and should be included (if members) in the list of the BSS candidates. Almost all the other objects considered in this region of the CMD can be explained as optical blends. This should be especially true for the 6 objects belonging to sub-group "c", but only new observations will provide a clear answer. If, however, these objects were indeed single stars belonging to the cluster, it would be important to understand their intrinsic nature. In the following Sect. 4.3.1 we present a possible scenario which relates these stars to the population of the BSS detected in the cluster.

Since BSS candidates were found to be close to the faint limiting magnitude in most plates used to obtain the bright star samples, and close to the saturation limit in most plates used for the faint samples, completeness was particularly difficult to achieve. In particular, the number of available measures for some BSS (and also for SGB stars at the same level of magnitude) is reduced occasionally to 2 or 3 plates. In order to improve the degree of completeness, independent searches of these objects have been carried out on different plates in each colour, and the list of candidate peaks detected in each independent search have been merged before performing the fitting procedure, in order to ensure that any possible candidate were measured whenever feasible. The smoothed distribution obtained for the SGB population at the same level of magnitude (see Fig. 11) testifies the reliability of this approach.

In conclusion, we believe that the quite irregular distribution of the stars along the BSS sequence is due to statistical fluctuations or to some residual incompleteness effect rather than to some intrinsic property of the stars, though we cannot exclude that this might indicate the existence of a multiple population of BSS of different origin. The large spread in colour may be intrinsic, somehow related to the formation mechanism, or due to photometric scatter from the unproper matching of measures taken at different phases of variability, since many BSS in other clusters show variability, and preliminary data seem to confirm that also some of the BSS in M 3 are variable (Nemec 1993, private communication).

4.2. Radial distributions

Nemec & Harris (1987), Nemec & Cohen (1989), Sarajedini & Da Costa (1991), Buonanno et al. (1990), Sarajedini (1992) and Ferraro et al. (1992c) found significant evidence in the loose clusters NGC 5053, NGC 5466, Ruprecht 106, NGC 6101, and NGC 5897 for a higher central concentration of the BSS in comparison to the other most populated branches. Similar evidences are present in other clusters whose study is still in progress (Sarajedini 1993).

Due to the very low stellar density in these clusters, BSS could be detected and measured even at the very centre. The analysis of the radial distribution is thus highly significant as it covers practically the entire size of the clusters. The high density of stellar images in the central regions of M 3 due both to the higher concentration of the cluster and to its larger total stellar population, prevented us from measuring BSS in the central re-

Table 13. List of blue stragglers and "special stragglers"

This paper					Sandage 1953 (SK 1982)		
Star	V	$(B-V)$	X	Y	Star	V	$(B-V)$
Bright sample							
10	17.77	0.12	122.	351.	II-II-29	17.89	0.04
11	17.30	0.20	156.	350.	I-II-21	17.39	0.06
58	17.77	0.48	159.	285.	–	–	–
96	17.47	0.10	-189.	244.	I-III-36	17.58	0.05
152	17.57	0.09	112.	202.	SK 201	17.50	0.26
211a	18.02	0.23	30.	168.	–	–	–
224	17.51	0.10	283.	159.	SK 62	17.43	0.28
382	17.37	0.18	-185.	103.	–	–	–
455a	17.76	0.39	-156.	70.	–	–	–
504	17.71	0.08	-207.	51.	–	–	–
698	17.87	0.47	127.	-25.	II-II-75	18.48	0.36
757	17.45	0.09	408.	-52.	II-VI-34	17.39	0.09
779	17.73	0.06	252.	-63.	SK 77	17.62	0.20
834	17.80	0.47	-95.	-85.	–	–	–
862	17.27	0.18	99.	-96.	–	–	–
954	17.65	0.45	-6.	-122.	–	–	–
1028	17.71	0.44	-33.	-147.	–	–	–
1127	17.36	0.19	8.	-201.	I-V-62	17.35	0.13
1185	17.77	0.08	-285.	-240.	II-IV-12	17.72	0.07
1222	17.69	0.12	11.	-287.	–	–	–
Faint sample							
314	18.15	0.38	24.	303.	II-II-37	18.16	0.38
531b	18.43	0.25	-114.	278.	–	–	–
638	18.85	0.33	141.	273.	–	–	–
1187s	18.99	0.32	61.	239.	–	–	–
1396	17.90	0.21	203.	230.	II-I-103	17.99	0.07
1519	18.33	0.30	-82.	222.	II-II-77	18.40	0.27
1729a	18.91	0.31	62.	213.	–	–	–
2763	18.35	0.34	-285.	157.	II-III-9	18.48	0.29
3281	18.16	0.34	292.	124.	–	–	–
3323a	18.85	0.32	-196.	118.	–	–	–
3427a	18.46	0.36	257.	111.	–	–	–
3454a	18.74	0.35	-191.	108.	–	–	–
3745	19.05	0.31	-196.	88.	–	–	–
3983	18.79	0.23	-263.	67.	–	–	–
4117a	18.52	0.24	-348.	53.	–	–	–
4119c	18.22	0.22	-286.	52.	–	–	–
4144a	18.54	0.28	-256.	51.	–	–	–
4400	18.45	0.25	312.	34.	–	–	–
4798b	19.10	0.30	279.	-1.	–	–	–
6110a	18.89	0.28	-177.	-116.	–	–	–
6137	18.22	0.25	-281.	-118.	–	–	–
6216	17.90	0.18	-206.	-127.	II-IV-64	17.86	0.14
7401a	18.70	0.30	154.	-211.	–	–	–
7654a	18.14	0.17	65.	-224.	–	–	–
7654b	18.62	0.36	66.	-225.	–	–	–
7704	17.81	0.08	-231.	-225.	I-IV-34	17.82	0.08
7956a	18.04	0.16	37.	-237.	I-V-42	18.11	0.01
8025a	18.15	0.38	33.	-241.	II-V-68	18.16	0.39

Table 13. (continued)

This paper					Sandage 1953 (SK 1982)		
Star	V	$(B-V)$	X	Y	Star	V	$(B-V)$
8121	18.65	0.33	233.	-244.	–	–	–
8381a	18.43	0.25	-73.	-262.	–	–	–
8484	18.09	0.12	55.	-266.	–	–	–
8552	18.77	0.26	70.	-270.	–	–	–
8573	18.69	0.33	104.	-272.	–	–	–
Faint sample, poor photometry							
1166s	19.14	0.28	-96.	239.	–	–	–
2028	18.80	0.18	70.	202.	–	–	–
2826	19.02	0.32	200.	155.	–	–	–
3336	19.07	0.26	-212.	117.	–	–	–
3432c	18.86	0.34	225.	112.	–	–	–
3483a	18.92	0.24	256.	106.	–	–	–
3575b	18.59	0.30	207.	100.	–	–	–
3902	18.86	0.32	244.	77.	–	–	–
3966a	18.57	0.36	-208.	68.	–	–	–
7904a	18.46	0.07	-164.	-235.	–	–	–
8075a	18.69	0.33	-156.	-245.	–	–	–
8456a	19.10	0.30	92.	-265.	–	–	–
Special stragglers (bright sample)							
131	17.48	0.59	101.	217.	–	–	–
383	17.00	0.61	-40.	102.	–	–	–
432a	17.53	0.56	160.	78.	–	–	–
631	16.95	0.55	-227.	4.	–	–	–
811	17.18	0.58	-168.	-74.	–	–	–
862a	17.43	0.60	101.	-96.	–	–	–
898	17.55	0.55	-79.	-104.	–	–	–
941	16.86	0.59	75.	-119.	–	–	–
972	16.55	0.55	378.	-127.	–	–	–
1157	16.65	0.52	-368.	-219.	–	–	–
1213	16.08	0.64	-274.	-273.	I-IV-40	16.07	0.52
1247	16.73	0.59	-175.	-312.	–	–	–
1255	17.07	0.59	91.	-323.	–	–	–

gions using the available photographic material. For this reason we could check the radial distribution of the BSS candidates only on the small annulus between 3.5′ and 6′ where the sample is complete for the full range in magnitude covered by the BSS. Over the larger square area AII the test can be performed only for the brightest objects ($B < 18.6$).

The BSS candidates of area "a" are shown in the XY-map of Fig. 18, where also other types of stars (i.e. HB, RGB, SGB and AGB) are marked in each panel for comparison.

Though not particularly striking, there is a weak indication for the BSS to be slightly less concentrated than the other stars, as already pointed out by Sandage (1953). Sandage & Katem (1982) noticed that, because the eight brightest BSS in the Sandage (1953, 1970) lists are not concentrated towards the cluster centre, they might alternatively be field stars. However, cluster membership was later confirmed for all of them, including the most distant candidate (*M 3-20* at about 13 arcmin from the cluster centre, Ables et al. 1982, Chaffe & Ables 1983), further supporting the suggestion that in the outer regions of M 3 there is a population of BSS which displays a cumulative radial distribution clearly not more centrally concentrated than normal stars in the same areas.

To quantify this indication we present in Fig. 19 the normalized cumulative radial distribution of the BSS , HB, AGB, and RGB stars over the whole mapped region for the objects brighter than $B = 18.6$ (the most significative and complete sample). In particular, a KS-test gives a full consistency between the distributions of HB, AGB, and RGB stars, and a 100% probability that the BSS are more spread out than RGB stars covering the same luminosity range. This result refers only to the rather narrow annulus in consideration, and cannot be extended straightforwardly to the entire area covered by the cluster, however the opposite conclusion (i.e. BSS more centrally concentrated than the other types of stars) is excluded by the present data.

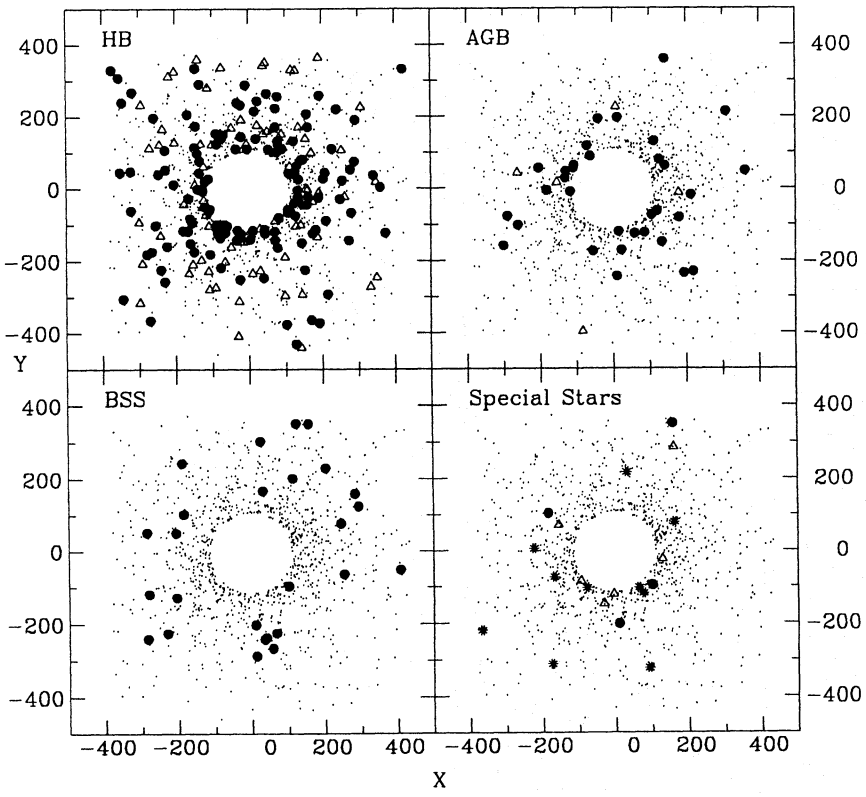

Fig. 18. XY maps of measured stars in the CBT sample. The *dots* represent RGB + SGB stars. In the HB, AGB, and BSS panels, *filled circles* mark these stars respectively, and *open triangles* are (known) variable objects. In the fourth panel the special stars discussed in Sect. 4 are identified with different symbols: *filled circles* = group "b" in Fig. 17, *open triangles* = group "c", *asterisks* = group "d"

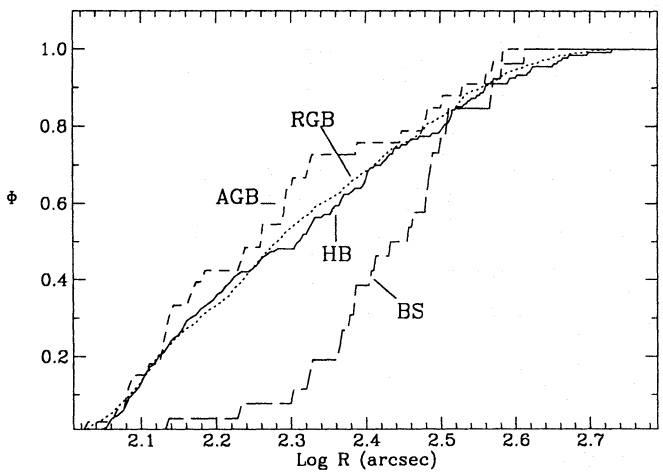

Fig. 19. Cumulative distributions as a function of radial distance for BSS-, HB-, SGB-, AGB-stars listed in the *Complete Bright Total* sample (CBT)

Figure 18 (bottom right panel) contains also a map where the positions in the cluster of the stars belonging to the subgroups "b", "c" and "d" in Fig. 17 are marked with different symbols. Since the number of objects in each set is small, the significance of radial trends, if any, cannot be quantified. For a more detailed discussion based on CCD data of a more central area see Ferraro et al. (1993).

4.3. BSS and stellar evolution

As widely discussed at the Workshop on "Blue Stragglers" (Livio & Saffer 1993), the interpretation of the BSS origin and evolution is still an open problem.

In synthesis, BSS may be (different types of) coalesced binaries or single stars. The major indication supporting their binary origin comes from the estimates of their present masses, $M(\mathrm{BSS}) \sim 1.3 \pm 0.3\,\mathrm{M}_{\odot}$, obtained mostly from the BSS detected in three globular clusters, namely NGC 5466 (Nemec & Harris 1987; Mateo et al. 1990), ω Cen (Da Costa & Norris 1988) and NGC 5053 (Nemec & Cohen 1989). These estimates are based on the pulsation properties of some BSS which exhibit variability, or on dynamical considerations (in these loose clusters the BSS are more centrally concentrated than normal stars). There is now a growing body of observational evidences (Frolov 1991; Bailyn 1992; Fusi Pecci et al. 1992) which suggest the possibility that different types of BSS (as far as origin and evolution are concerned) may exist in different clusters and even in different regions of the same cluster.

Here we want to explore whether evolved BSS can be detected in the CMD of globular clusters (M 3 in particular). Since we shall base our considerations on evolutionary models of normal stars, it is important to stress the caveat, pointed out for instance by Ostriker (1992, see Fusi Pecci et al. 1993a), that "if formed by either merging or collision, BSS should rotate *very* rapidly and then will evolve in a totally different way from normal stars". On the other hand, as noted by Da Costa (1992, see Fusi Pecci et al. 1993a) "spectra of BSS in ω Cen do not show any indication of rotation (at least in surface layers) velocities as

high as 100's of km s^{-1}. Hence, either a braking mechanism is at work (at least for the outer layers), or the mechanisms of BSS formation from binaries are still not well understood (unless BSS come from single stars?).

We briefly analyse two possible ways of detecting post-BSS in M 3.

4.3.1. Between the TO and the SGB

As we have anticipated in Sect. 4.1, we favour the "photometric" interpretation for most of the peculiar stragglers, however in principle the following "evolutionary connection" is also possible.

The stars in the groups "b" and "c", and at least some of those in group "d" in Fig. 17, could delineate an evolutionary track for the post-BSS evolution. In particular, the 4 stars in group "b" might be slightly evolved BSS representing the turnover at high luminosity of the BSS sequence. Note that a similar feature is also visible in the CMD of NGC 5053 (Field 1, Fig. 2 in Nemec & Cohen 1989). The 6 stars in group "c" would be the clump at the base of the RGB predicted theoretically for stars in the mass range 1.3–1.5 $M_\odot$ (Castellani et al. 1992). The relative minimum in luminosity in the tracks at the base of RGB is due to the envelope runaway expansion and is a strong function of metallicity, in the sense that the luminosity difference with respect to the relative maximum reached after the MS turnoff increases with increasing metallicity. Finally, some of the sparse stars located in the region "d", could be post-BSS evolving along the early RGB, while the later evolutionary phases would produce objects indistinguishably mixed with the normal RGB stars.

Among the various sets of isochrones for TO masses in the range 1–2 $M_\odot$ one can easily find a locus which provides a nice *qualitative* fit of the points. Just to show an example, we report in Fig. 20 two isochrones computed by Castellani et al. (1992, their Table 3) assuming $Y = 0.23$, $Z = 0.02$, and age = 2, 3 and 16 Gyr, which have been arbitrarily shifted by 0.20 mag in colour to yield an apparently fair matching to the data. Since tracks with a more suitable metallicity are not presently available, this example cannot be taken as a proper description of the data. New specific tracks with the appropriate metallicity are necessary for this type of analysis and would be very welcome. A *quantitative* best fit is much more difficult to obtain. One should in fact match at the same time the overall shape of the star distributions, the relative numbers of stars compared to the respective evolutionary lifetimes, and the absolute location of the observed and theoretical loci for the assumed chemical composition. On the other hand, it is not obvious at all that the chemical composition, assumed as the same as for the other normal stars in the cluster, is adequate also for a BSS formed via any type of dynamical interaction of two (or more) stars, or via peculiar mixings in a single star. Indeed, there is some indication that the BSS ridge lines are increasingly redshifted away from the extension of their original MS with increasing metallicity (Fusi Pecci et al. 1992). The *dashed line* in Fig. 20 represents the ZAMS of the Pleiades (Walker 1985), properly shifted to match the faint MS in M 3, and the BSS do not appear as just "normal" ZAMS stars more massive than the corresponding TO objects.

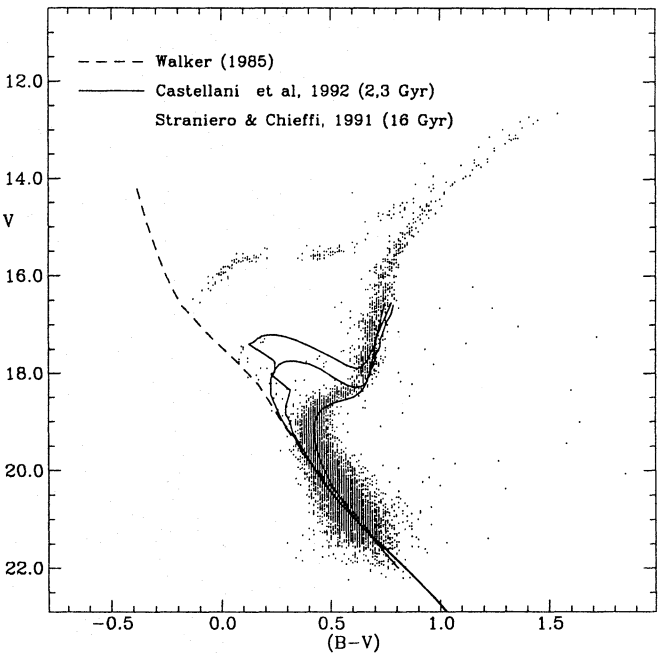

Fig. 20. The *full lines* report three isochrones computed by Castellani et al. (1992, Table 3) assuming $Y = 0.23$, $Z = 0.02$, and age (top to bottom) 2, 3 and 16 Gyr arbitrarily shifted by 0.20 mag in colour to show how a *purely qualitative* matching with the stars included in the groups "a", "b", "c", and "d" in Fig. 17 could perhaps be obtained. The *dashed line* represents the ZAMS of the Pleiades (Walker 1985), properly shifted to match the faint MS

4.3.2. On the HB

Since it has been shown quite convincingly that BSS are more massive than normal MS stars, and that rotation does not seem to be so important as to alter significantly the BSS single-star characteristics, they are expected to evolve sooner or later into core helium burning objects more massive than the normal HB stars, as first pointed out by Renzini (and reported in Renzini & Fusi Pecci 1988, and discussed in detail by Fusi Pecci et al. 1992). They would then be indistinguishable from the other cluster members during most of their life across the CMD, but may become detectable during the longest and best located evolutionary stages like the ZAHB.

They might be detected in principle also during some short-lived but observationally "outstanding" evolutionary phase, such as the late stages of both the RGB and AGB evolution (Greggio & Renzini 1990; Renzini & Greggio 1990) and the Anomalous Cepheid phase. Being more massive, they would predominantly populate the uppermost part of the RGB and AGB or even reach a brighter magnitude than the typical level for normal stars. There are observational evidences which may support this scenario (Whitelock et al. 1991; Freedman 1992). As far as the Anomalous Cepheids are concerned, it is inter-

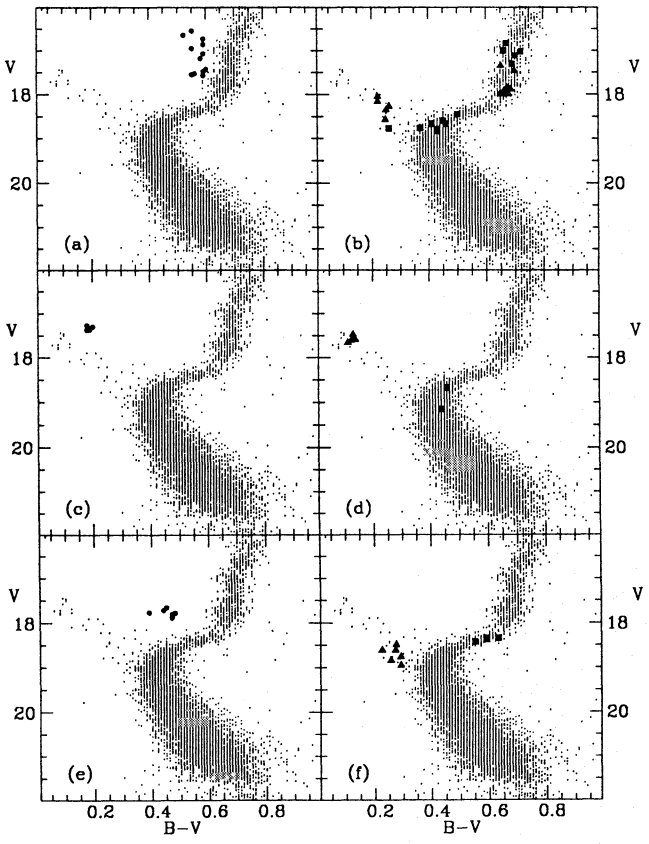

Fig. 21a–f. Optical blends and "true" BSS and BSS-descendant candidates. The stars marked as *filled circles* in the left panels are interpreted as due to the blend of a star marked a *filled triangle* + a star marked as a *filled square* in the corresponding right panels (Sect. 4.4.2)

esting to note that the only such star found in globular clusters belongs to the loose cluster NGC 5466, which is very rich in BSS (Zinn & King 1982; Nemec & Harris 1987; Mateo et al. 1990).

A BSS-progeny could also be detected on the ZAHB. Adopting $M_{BSS} \sim 1.3\,M_{\odot}$ as typical for the BSS population of M 3, and assuming that mass loss prior to the core helium ignition would not exceed the values predicted by most of the current mechanisms (i.e. total mass lost not larger than ~ 0.3–$0.4\,M_{\odot}$), the helium-core burning daughter of a BSS in M 3 is therefore expected to be a star with total mass close to $1\,M_{\odot}$, which would lie on the red extension of the ZAHB (Seidl et al. 1987; Sweigart et al. 1987). In this context it is then important to consider the 7 ER stars we singled out while discussing the HB morphology in Sect. 3.3.3. Although these stars represent a fluctuation of only $\sim$ 10–15% with respect to the normal observed RHB population in M 3, similar stars can be found in almost all the clusters with a significant BSS population, and can be detected even in several dwarf spheroidal galaxies rich in BSS and Anomalous Cepheids. Their interpretation as normal red HB stars cannot be totally excluded, however the possibility that they are indeed the evolved progeny of the BSS is to be taken into serious account, as the evidence in this sense is growing stronger.

The overall scenario emerging from the analysis of 23 Galactic globular clusters, the pros and cons of this new interpretative framework, and the BSS Luminosity Functions have been presented and discussed in detail in a previous paper (Fusi Pecci et al. 1992) to which we refer the interested reader.

Acknowledgements. This study would not have been possible without the kindness of Allan Sandage who lent us the plates, and encouraged and supported our work with many helpful comments and suggestions during all these years. It is our pleasure to thank him warmly.

We are also very grateful to Alvio Renzini who inspired the essence of this work and continuosly urged us to present these data and pursue this global project.

Finally, we are indebted to Robert Kraft, Mario Mateo, Alvio Renzini, Bob Rood and Allan Sandage for reading various versions of an original massive paper now broken down into more tractable parts.

This work was supported by the *Gruppo Nazionale di Astronomia* (GNA) of the *Consiglio Nazionale delle Ricerche* (CNR), by the *Ministero della Pubblica Istruzione* (MPI), and by the *Consiglio per le Ricerche Astronomiche* (CRA) of the *Ministero per l' Università e la Ricerca Scientifica* (MURST).

References

Ables H.D., Dahn C.C., Hewitt A.V., 1982, PASP 94, 748
Aurière M., Cordoni J.P., 1983, A&AS 52, 383
Aurière M., Ortolani S., Lauzeral C., 1990, Nat 344, 638
Bailyn C.D., 1992, ApJ 392, 519
Bailyn C.D., Grindlay J.E., Cohn H., Lugger P.M., 1988, ApJ 331, 301
Bailyn C.D., Grindlay J.E., Cohn H.N., et al., 1989, AJ 98, 882
Bailyn C.D., Iben I.Jr., 1989, ApJ 347, L21
Bergbush P.A., VandenBerg D.A., 1992, ApJS 81, 163
Bertola F., Burstein D., Buson L.M., Renzini A., 1993 (preprint)
Bica E.D.L., Pastoriza M.G., 1983, Ap&SS 91, 99
Bonifazi A., Fusi Pecci F., Romeo G., Tosi M., 1991, MNRAS 245, 15
Bressan A., Bertelli G., Chiosi C., 1986, Mem.SAIt 57, 411
Brodie J.P., Hanes D.A., 1986, ApJ 300, 258
Buonanno R., Buscema G., Corsi C.E., Iannicola G., Fusi Pecci F., 1983a, A&AS 51, 83
Buonanno R., Buscema G., Corsi C.E., Ferraro I., Iannicola G., 1983b, A&A 126, 278
Buonanno R., Buscema G., Fusi Pecci F., Richer H.B, Fahlman G.G., 1990, AJ 100, 1811
Buonanno R., Buzzoni A., Corsi C.E., Fusi Pecci F., Sandage A.R., 1986, Mem.SAIt 57, 391
Buonanno R., Buzzoni A., Corsi C.E., Fusi Pecci F., Sandage A.R., 1988, in: Grindlay J.E., Philip A.G.D. (eds.) Globular Cluster Systems in Galaxies, Reidel, Dordrecht, p. 621
Buonanno R., Cacciari C., Corsi C.E., Fusi Pecci F., 1990, A&A 230, 315
Buonanno R., Caloi V., Castellani V., et al., 1986, A&AS 66, 79
Buonanno R., Corsi C.E., De Biase G.A., Ferraro I., 1979, in: Sedmak G., Capaccioli M., Allen R.J. (eds.) Image Processing in Astronomy, Trieste, Italy, p. 354
Buonanno R., Corsi C.E., Fusi Pecci F., Alcaino G., Liller W., 1984, A&AS 57, 75
Buonanno R., Corsi C.E., Fusi Pecci F., 1985, A&A 145, 97 (BCF85)
Buonanno R., Corsi C.E., Fusi Pecci F., 1989, A&A 216, 80 (BCF89)
Buonanno R., Iannicola G., 1988, PASP 101, 294
Burstein D., McDonald L.H., 1975, AJ 80, 17

Burstein D., Bertola F., Buson L., Faber S.M., Lauer T.R., 1988, ApJ 328, 440
Buzzoni A., Cacciari C., Fusi Pecci F., Buonanno R., Corsi C.E., 1992, A&A 254, 110
Buzzoni A., Fusi Pecci F., Buonanno R., Corsi C.E., 1983, A&A 123, 94 (BFBC)
Buzzoni A., et al. 1994a (in preparation)
Buzzoni A., et al. 1994b (in preparation)
Cacciari C., et al. 1994 (in preparation)
Cannon R.D., 1981, in: Philip A.G.D., Hayes D.S. (eds., Astrophysical Parameters for Globular Clusters, IAU Coll. No. 168, Schenectady, L. Davis Press Inc., p. 501
Carney B.W., Storm J., Jones R.V., 1992, ApJ 386, 663
Castellani V., Chieffi A., Pulone L. 1989, ApJS 76, 911
Castellani V., Chieffi A., Pulone L. 1991, ApJ 344, 239
Castellani V., Chieffi A., Straniero O., 1992, ApJS 78, 517
Castellani V., Chieffi A., Pulone L., Tornambè A., 1985, ApJ 296, 204
Cederbloom S., Moss M., Cohn H., et al., 1992, AJ 103, 480
Chaboyer B., Sarajedini A., Dermarque P., 1992, ApJ 394, 515
Chaffee F.H.Jr., Ables H.D., 1983, PASP 95, 835
Chieffi A., Straniero O., 1989, ApJS 71, 47
Crocker D.A., Rood R.T., O'Connell R.W., 1988, ApJ 332, 236
Cudworth K.M., 1979, AJ 84, 1312.
Da Costa G.S., Norris J., 1988, in: Grindlay J.E., Philip A.G.D. (eds.) Globular Cluster Systems in Galaxies, Reidel, Dordrecht, p. 681
Da Costa G.S., Villumsen J.V., 1981, in: Philip A.G.D., Hayes D.S. (eds.) Astrophysical Parameters for Globular Clusters, Schenectady, L. Davis Press Inc, p. 527.
Davidsen A.F., Ferguson H.C., 1992, in: Thuan T.X., Balkowski C., Van J.T.T. (eds.) Physics of Nearby Galaxies: Nature or Nurture?, Edtions Frontiers, Paris (in press)
Djorgovski S.G., Piotto G., 1992, AJ 104, 2112
Djorgovski S.G., Piotto G., King I.R., 1988, in: Merritt D. (ed.) Dynamics of Dense Stellar Systems, Cambridge University Press, Cambridge, p. 147
Djorgovski S.G., Piotto G., Mallen-Ornellas G., 1991a, in: Janes K. (ed.) Formation & Evolution of Star Clusters, A.S.P. Conference Series No. 13, p. 262
Djorgovski S.G., Piotto G., Phinney E.S., Chernoff D.F., 1991b, ApJ 372, L41
Dorman B., Rood R.T., 1992 (preprint)
Drukier G.A., Fahlman G.G., Richer H.B., 1989, ApJ 342, L27
Eggen O.J., Sandage A.R., 1969, ApJ 158, 669
Ferraro F.R., Clementini G., Fusi Pecci F., Buonanno R., Alcaino G., 1990, A&AS 84, 59 (NGC 2808)
Ferraro F.R., Clementini G., Fusi Pecci F., Buonanno R., 1992a, MNRAS 252, 357 (NGC 6171)
Ferraro F.R., Clementini G., Fusi Pecci F., Sortino R., Buonanno R., 1992b, MNRAS 256, 391 (NGC 1904)
Ferraro F.R., Fusi Pecci F., Buonanno R., 1992c, MNRAS 256, 376 (NGC 5897)
Ferraro F.R., et al., 1994 (in preparation)
Ferraro F.R., Fusi Pecci F., Cacciari C., et al., 1993, AJ 106, 2324
Ferraro F.R., Paresce F., 1993, AJ 106, 154
Freedman W., 1992, AJ 104, 1349
Frogel J.A., Cohen J.G., Persson S.E., 1983, ApJ 275, 773
Frolov M.S., 1991, IBVS, 3566
Fusi Pecci F., 1987, in: Philip A.G.D., Hayes D.S., Liebert J. (eds.) Second Conference on Faint Blue Stars, Schenectady, L.Davis Press, p. 107
Fusi Pecci F., Renzini A. 1978, in: Philip A.G.D., Hayes D.S. (eds.) The HR Diagram, Reidel, Dordrecht, p. 225
Fusi Pecci F., Cacciari C., Ferraro F.R., 1993a, in: Meylan G., Djorgovski G.S. (eds.) Dynamics of Globular Clusters: A Workshop in Honor of Ivan, R. King, ASP Series, Vol. 50, 217
Fusi Pecci F., Ferraro F.R., Crocker D.A., Rood R.T., Buonanno R., 1990, A&A 238, 95
Fusi Pecci F., Ferraro F.R. , Corsi C.E., Cacciari C., Buonanno R., 1992, AJ 104, 1831
Fusi Pecci F., Ferraro F.R., Bellazzini M., et al., 1993b, AJ 105, 1145
Geisler D., 1984, ApJ 287, L85
Gingold R.A., 1974, ApJ 193, 177
Gingold R.A., 1976, ApJ 204, 116
Green E.M., Demarque P., King C.R., 1987, The Revised Yale Isochrones and Luminosity Functions, New Haven, Yale Obs. Pub.
Greggio L., Renzini A., 1990, ApJ 364, 35
Grindlay J.E., Gurski H., Parsignault D.R., et al., 1981, in: Philip A.G.D., Hayes D.S. (eds.) Astrophysical Parameters for Globular Clusters, IAU Coll. No. 168, L. Davis Press, Schenectady, p. 477
Guarnieri M.D., et al., 1994, (in preparation)
Guarnieri M.D., Longmore A.J., Fusi Pecci F., Dixon R.I., 1990, Mem-SAIt 61, 143
Iben I.Jr., 1968, Nat 220, 143
Iben I.,Jr., 1990, ApJ 353, 215
Iben I.Jr., Tutukov A.V., 1986, ApJ 311, 753
Kadla Z.I., Gerashchenko A.N., 1982, Astr. Tsirk. No. 1123, 1
Kraft R.P., Sneden C., Langer G.E., Prosper C.F., 1992, AJ 104, 645
Kron G.E., Guetter H.H., 1976, AJ 81, 817
Kurucz R.L., 1979, ApJS 40, 1
Lauzeral C., Aurière M., Ortolani S., Melnick J., 1992, A&A 263, 63
Lee Y.W., 1992, AJ 104, 1780
Lee Y.W., Demarque P., Zinn R.J., 1990, ApJ 350, 155
Livio M., Saffer R., 1993, eds., in: Blue Stragglers, Workshop, STScI, Oct. 13–14, 1992, ASP Conf. Series, Vol. 53
Lutz T.E., Hanson R.B., van Altena W.F., 1987, BAAS 19, 675
Mateo M., Harris H.C., Nemec J.M., Olszewski E.W., 1990, AJ 100, 469
Mengel J.E., Norris J.E., Gross P.G., 1976, ApJ 204, 488
Nemec J.M., Cohen J.G., 1989, ApJ 336, 780
Nemec J.M., Harris H.C., 1987, ApJ 316, 172
Paez E., Straniero O., Martinez Roger C., 1990, A&AS 84, 481
Paresce F., Shara M., Meylan G., et al., 1991, Nat 352, 297
Peterson C.J., 1986, PASP 98, 192
Pilachowski C.A., 1984, ApJ 281, 614
Piotto G., King I.R., Djorgovski S., 1988, AJ 96, 1918
Ratnatunga K.U., Bahcall J.N., 1985, ApJS 59, 63
Reed B.C., Hesser J.E., Shawl S.J., 1988, PASP 100, 545
Renzini A., 1977, in: Bouvier P., Maeder A. (eds.) Advanced Stages in Stellar Evolution, Geneva Obs., p. 149
Renzini A., 1983, Mem.SAIt 54, 335
Renzini A., Fusi Pecci F., 1988, ARA&A 26, 199
Renzini A., Greggio L., 1990, in: Jarvis B.J., Terndrup D.M. (eds.) Bulges of Galaxies, ESO-CTIO Workshop, Garching, ESO, p. 47
Rood R.T., Crocker D.A., 1985a, in: Philip A.G.D. (ed.) Hot Population II Stars, L. Davis Press, Schenectady, p. 99
Rood R.T., Crocker D.A., 1985b, in: Danziger I.J., Matteucci F., Kjar K. (eds.) Production and Distribution of CNO Elements, Garching, ESO, p. 61
Rood R.T., Crocker D.A., 1989, in: Schmidt E.G. (ed.) The Use of Pulsating Stars in Fundamental Problems of Astronomy, IAU Coll. No. 111, Cambridge University Press, Cambridge, p. 103

Salaris M., Chieffi A., Straniero O., 1993 (preprint)
Sandage A.R., 1953, AJ 58, 61
Sandage A.R., 1970, ApJ 162, 841
Sandage A.R., 1982, ApJ 252, 553
Sandage A.R., 1990, ApJ 350, 603 (S90)
Sandage A.R., 1993a, AJ 106, 687
Sandage A.R., 1993b, AJ 106, 703
Sandage A.R., 1993c, AJ 106, 719
Sandage A.R., Cacciari C. 1990, ApJ 350, 645
Sandage A.R., Katem B., 1977, ApJ 215, 62
Sandage A.R., Katem B., 1982, AJ 87, 537
Sandage A.R., Katem B., 1983, AJ 88, 1146
Sandage A.R., Smith L.L., 1966, ApJ 144, 886
Sandage A.R., Wallerstein G., 1960, ApJ 131, 598
Sarajedini A., 1992, AJ 104, 178
Sarajadeni A., 1993, in: Livio M., Saffer R. (eds.) Blue Stragglers, Workshop, STScI, Oct. 13–14, 1992, ASP Conf. Series, Vol. 53, 14
Sarajedini A., Da Costa G.S., 1991, AJ 102, 628
Sarajedini A., King C.R., 1989, AJ 98, 1624
Seidl E., Demarque P., Weinberg D., 1987, ApJS 63, 917
Smith H.A., 1984, ApJ 281, 148
Stetson P.B., 1991, in: Philip A.G.D., Upgren A.R., Janes K. (eds.) Precision Photometry: Astrophysics of the Galaxy, L. Davis Press, Schenectady, p. 69
Straniero O., Chieffi A., 1991, ApJS 76, 525
Stringfellow G.S., Bodenheimer P., Noerdlinger P.D., Arigo R.J., 1983, ApJ 264, 228
Sweigart A.V., Gross P.G., 1976, ApJS 32, 367
Sweigart A.V., Renzini A., Tornambè A., 1987, ApJ 312, 762
Thomas P., 1989, MNRAS 238, 1319
van Albada T.S., Baker N., 1971, ApJ 169, 311
VandenBerg D.A., Bell R.A., 1985, ApJS 58, 561
VandenBerg D.A., Poll H.E., 1989, AJ 98, 1451
VandenBerg D.A., Bolte M., Stetson P.B., 1990, AJ 100, 445
Walker A.R., 1985, MNRAS 213, 889
Walker A.R., 1992, ApJ 390, L81
Whitelock P., Feast M., Catchpole R., 1991, MNRAS 248, 276
Zinn R.J., King C.R., 1982, ApJ 262, 700
Zinn R.J., West M.J., 1984, ApJS 55, 45